Original Research Article

International journal of spray and combustion dynamics

International Journal of Spray and Combustion Dynamics
2017, Vol. 9(1) 19–43

DOI: 10.1177/1756827716652474
journals.sagepub.com/home/scd
SAGE

A systems perspective on non-normality in low-order thermoacoustic models: Full norms, semi-norms and transient growth

Ralf S Blumenthal[1,4], Arun K Tangirala[2], RI Sujith[3,4] and Wolfgang Polifke[1]

Abstract

Non-normal transient growth of energy is a feature encountered in many physical systems. Its observation is intimately related to the norm used to describe the system dynamics. For a multi-physics problem such as thermoacoustics, where a heat source is in feedback with acoustic waves and a flow field, the appropriate metric is an ongoing matter of debate. Adopting a systemic perspective, it is argued in the present paper that an energy norm is, in principle, a matter of choice, but one that is critically tied to the dynamics described by the system model. To illustrate our arguments, it is shown that different norms exhibit the non-normal dynamics of thermoacoustic systems differently, but that this difference is fully explicable by the energy flux and source terms related to the formulation of the model. The non-normal dynamics as such is unaffected by the choice of norm, and transient growth merely results from a maximization of the flux and source terms governing the energy balance associated with the specific model formulation. Investigating transient growth for arbitrary energy norms requires the capability to handle semi-norm optimization problems. In the present study, we propose an approach to do so using the singular value decomposition. Non-normal transient growth around a stable fix point is then investigated for a low-order model of a simple thermoacoustic configuration of a premixed flame enclosed in a duct with non-zero mean temperature jump and bulk mean flow. The corresponding optimal mode shapes and pertinent parameters leading to transient growth are identified and discussed. For transient growth resulting from the interaction of the flame with the acoustic field, it is found that heat sources with a fast response lead to more transient growth than slow heat sources, because the system can bear a larger source term before becoming linearly unstable. Furthermore, the amount of transient energy growth does not increase monotonically with the amplitude of the initial perturbation of the flame.

Keywords

Non-normality, transient growth, energy norm, semi-norm, thermoacoustics

Date received: 9 May 2014; accepted: 25 March 2016

Motivation and scope

Energy norms are the foundation to investigating transient growth of perturbation energy resulting from non-normal processes in any kind of system. A norm is required to find the so-called optimal initial condition (OIC) by solving an optimization problem with the energy norm as cost function.[1] The OIC is the system state that leads to maximum possible transient amplification $G_{\max}$ of a stable, linear, autonomously evolving system. The concepts of non-normality and transient growth of perturbation energy were successfully employed in hydrodynamics in the context of non-modal stability analysis. The first major works were published in the 1990s[1–7] in response to the insufficiencies exhibited by modal linear stability analysis (classical linear spectral analysis).

[1]Professur für Thermofluiddynamik, TU München, Garching, Germany
[2]Department of Chemical Engineering, IIT Madras, Chennai, India
[3]Department of Aerospace Engineering, IIT Madras, Chennai, India
[4]Institute for Advanced Study, TU München, Garching, Germany

Corresponding author:
Ralf S Blumenthal, Professur für Thermofluiddynamik, TU München, Boltzmannstr. 15, D-85748 Garching, Germany.
Email: ralf.blumenthal@tum.de

Ideas of non-normality were applied to thermoacoustic problems only a few years ago by Balasubramanian & Sujith[8–10] and by Kedia et al.,[11,12] and have since attracted the interest of other researchers.[13–18] Juniper[15,16,19] has shown that thermoacoustic triggering from small-amplitude perturbations may follow a path similar to that in bypass transition to turbulence. Non-normal effects can transiently amplify perturbations of low energy around an unstable oscillating limit cycle before the perturbations are repelled towards the undesired stable oscillating limit cycle by the action of nonlinearities. The scenario of triggering thus happens via the combined effect of non-normality and nonlinearity, which both contribute to the growth of perturbations. This is where triggering in thermoacoustics fundamentally differs from bypass transition to turbulence. For the latter, the nonlinear terms redistribute energy in a conservative manner, and growth is solely due to non-normal effects, which are purely linear.[1,20,21] In thermoacoustics, provided linear acoustics, the nonlinearity arises from the fluctuating heat source, which is a non-conservative source term.

Results of any non-normal analysis are subject to the particular energy norm used for optimization. For internal non-reacting flows, the kinetic energy of the perturbations is obviously a relevant energy metric, and the role of non-normality is beyond dispute.[1,6] However, if a system consists of multiple subsystems in feedback, it may not be evident which energy norm represents a pertinent measure of the system dynamics. This is the case for thermoacoustic systems, where a heat source subsystem is in feedback with an acoustics subsystem and/or a flow subsystem. Discussions about the appropriate energy norm are an ongoing matter of debate.[13,14,17,22,23] For example, Wieczorek et al.[17] report that there can be differences in $G_{\max}$ of several orders of magnitude when investigating the same non-isentropic thermoacoustic system subject to different energy norms. George and Sujith[22,23] attempt to shed light on the quality of different existing energy norms by qualifying their respective mathematical properties. Due to these issues, the role of non-normality in thermoacoustics is neither unambiguously demonstrated (also due to the lack of experimental evidence) nor generally accepted.[24]

To contribute to the ongoing discussions on the proper choice of norm in the field of thermoacoustics, the present study addresses two main points. Since an energy norm is one of several means to quantify the dynamics of a system model by a scalar measure, the first objective consists in demonstrating that there are no unique, proper energy norms. This is demonstrated by the example of two low-order thermoacoustic models. The second objective is to analyze the dynamics and the relevant parameters influencing non-normal transient growth around a stable fix point. Both objectives are introduced in more detail in the following.

Regarding the first objective, it is highlighted in the present study that an energy norm is, in principle, a matter of choice that is critically tied to the dynamics described by the system model. As integral part of the model definition, the energy norm prescribes the way the system dynamics manifests itself to the investigator and thus how the results should be interpreted. In this sense, the question of appropriate energy norm should be restated as a question of appropriate *perspective* (''you get what you ask for''). There certainly exist perspectives that may be more or less reasonable to analyze a given situation. That is, some energy norms may suggest a misleading conclusion or an incomplete picture, whereas others may not.

The ongoing discussion in the thermoacoustic literature seems to be strongly influenced by the term perturbation *energy*, which suggests a physical and conserved quantity. This is clearly inappropriate for linearized fields that interact with a stationary base. Also, energy norms are many times sought and used with the aim of representing a quantity that allows to reliably assess the stability of a thermoacoustic system.[25–29] For an energy norm to be ''mathematically consistent,'' Giauque et al.[30] and George and Sujith[23] require that an energy norm ''should not support spurious energy growth or decay in the absence of physical sources or sinks of energy''.[23,31] The problem with this requirement lies in the fact that any energy norm evolves in time according to the sources and sinks that originate from its definition. Whether or not such sources or sinks are rated as physical or spurious is thus a matter of subjective assessment, and depends on the model definition in the first place. In contrast, the present study adopts a systems-based perspective, where an energy norm is generically defined as the L_2-norm of the output of the system model. In the following, we therefore use the term *output energy* instead of energy norm. The output, in turn, is a function of the states of the model, and can be chosen as part of the definition of the model. Once the model is defined (that is, the dynamics and the output), the temporal evolution of output energy is unambiguously given, and can be interpreted accordingly.

To illustrate our arguments regarding the choice of output, we analyze two thermoacoustic setups with respect to the observed levels of non-normal transient growth: the above mentioned model studied by Wieczorek et al.,[17] and a fluctuating heat source enclosed in a one-dimensional duct. In all cases, inspection of the net balance of flux and source terms associated with the definitions of output sheds light on the observed non-normal dynamics. Whether the observed dynamics matches physical intuition is a different question. However, it becomes clear that the choice of

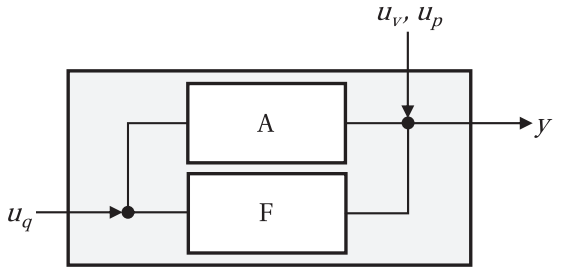

Figure 1. Systems sketch of the present thermoacoustic system, in which the acoustics/flow subsystem (index *A*) is in permanent feedback with the flame subsystem (index *F*). The output of the thermoacoustic system is denoted by *y*, and u_i signifies the individual inputs to the respective states of the subsystems. These are spatially distributed acoustic variables of velocity *v* and pressure *p* for the acoustics subsystem, and additional states representing the fluctuating heat release rate *q* for the flame subsystem.

output does not alter the dynamics as such (i.e. the temporal evolution of the state vector).

As mentioned above, the second objective of the present study is to analyze the dynamics and the relevant parameters influencing non-normal transient growth around a stable fix point. To this aim, we investigate a simple thermoacoustic system inspired by the classical Rijke tube. A perfectly premixed flame is enclosed in a one-dimensional duct with a bulk mean flow. The heat source causes a constant mean temperature jump at the position of the flame. The thermoacoustic system thus consists of two subsystems: the acoustics/flow subsystem (index *A*) with states representing the spatially distributed values of acoustic velocity *v* and pressure *p*, and the flame subsystem (index *F*) with states representing the fluctuating heat source. Both subsystems are in permanent feedback, as indicated by the schematic diagram shown in Figure 1. The overall system produces an output *y*, and the states of both subsystems can be individually forced by inputs u_i. The dynamics of the acoustics/flow subsystem is approximated by a method of weighted residuals (MWR), which may be more familiar to the reader as Galerkin method. The dynamics of the flame subsystem is modeled by an impulse response filter model derived in Blumenthal et al.[32] Since the output is a matter of choice, we decide to measure the dynamics of the model by defining the output energy to correspond to the acoustic energy with mean flow (sometimes referred to as Cantrell and Hart norm[33]). In this case, the output only contains contributions from the states of the acoustics subsystem, and the output energy defines a semi-norm.

Determining $G_{\max}$ subject to a semi-norm describes an ill-posed optimization problem. If the magnitude of the states not contained in the definition of the output is unbounded, it can result in infinite growth of output energy. This is because the nullspace of a semi-norm extends beyond the trivial nullvector.[34] Semi-norm optimization is well defined only if the nullspace defined by the semi-norm is bounded. This topic is addressed by Foures et al.[34] in the framework of variational methods, and recently also by Magri.[35] However, most of the studies on transient growth in thermoacoustics make use of the singular value decomposition (SVD) to optimize for optimal growth of output energy, because it is computationally inexpensive and easy to implement. Using SVD, it is not possible to add constraints that would account for bounded nullspaces of semi-norms. In the present study, we propose an approach to overcome this issue and to perform semi-norm optimization using SVD. As will be shown in the Optimization of output energy using SVD section, the concept of $G_{\max}$ is extended from autonomous to forced systems. It thereby becomes possible to constrain the magnitude of the states not included in the output. To the authors' knowledge, the only other study related to this matter is a paper by Jiménez,[36] where semi-norm optimization is used to investigate spatially localized energy amplification in turbulent channel flows.

The fact that the present study investigates transient growth subject to a semi-norm marks the main difference to previous studies on non-normality in thermoacoustics, where the output energies correspond to the weighted L_2-norm of the state vector of the system model. In this case, the output energy conveniently represents a full norm, and the optimization leading to $G_{\max}$ is well posed. For example, the states of the thermoacoustic model of Mariappan and Sujith[37] resolve fluctuations in entropy and the model contains mean flow effects, such that they use Chu's norm[31] and Myer's norm,[38] respectively. Juniper's thermoacoustic model[15,16] consists of acoustic states without mean flow, and the output energy is given by the acoustic energy. The latter three energies are derived from first principles, and therefore correspond to generic forms of perturbation energy: kinetic, potential and internal perturbation energy. Other studies introduce additional states to model the heat source subsystem.[8,13,14] In these cases, the output energies do not necessarily correspond to a generic form of perturbation energy. For instance, Subramanian and Sujith[13] define the flame states such that the output energy can be interpreted as acoustic energy plus a contribution from acoustic monopole sources distributed along the flame surface.

Semi-norm optimization is an important element with regards to retaining a maximum degree of flexibility in choosing the output. It also necessitates to analyze another parameter in the optimization procedure. The amount of perturbations initially contained in the states that are not accounted for in the output energy certainly has an effect on the observable amount of maximum transient growth. For the flow system

investigated by Foures et al.,[34] transient growth of kinetic perturbation energy in the flow subsystem increases monotonically with the amount of perturbations initially contained in the subsystem of viscosity, because the energy transfer is conservative. For the simple thermoacoustic system analyzed in the present study, the situation is different. As will be shown in The dynamics of non-normal transient growth section, the level of maximum transient growth of acoustic energy is not a monotonically increasing function of the amplitude of the initial perturbation of the flame, because the acoustic field needs to be receptive to fluctuations in heat release rate in order to increase the level of acoustic energy.

For the limiting case of zero initial perturbations in the flame subsystem, we analyze the effect of different parameters such as temperature jump, mean flow, flame position, etc. on the maximum level of transient growth. It is found that the ratio of time scales between the flame subsystem and acoustics is an important factor. Flames with fast response times lead to much higher levels of transient growth than slow flames. This is because thermoacoustic system with fast heat sources can withstand a stronger Rayleigh term before becoming linearly unstable. Further, the mode shapes leading to maximum transient growth are discussed in the context of short-term maximization of source and flux terms. It thereby once more becomes evident that non-normal transient growth is fully explicable by inspection of the energy balance associated with the definition of the system model.

The paper is structured as follows. The thermoacoustic model is introduced in The low-order thermoacoustic model section, where we also define the reference configuration that will be analyzed throughout the paper. The Discussion of output energy section then deals with the first objective of the present work, which is to show that the output can be chosen as an arbitrary function of the states of the system model. Observed levels of maximum transient growth are explained in view of the resulting flux and source terms associated with the model definition. Subsequently, we lay out the approach of performing semi-norm optimization using SVD (see the Optimization of output energy using SVD section). The Analysis of non-normal transient growth around a stable fix point section finally treats the second objective of the present work, which is to analyze the dynamics and relevant parameters of non-normal transient growth around a stable fix point in the simple thermoacoustic system introduced in The low-order thermoacoustic model section. Conclusions are given in the last section.

The low-order thermoacoustic model

The current section introduces the low-order thermoacoustic model formulation used in the present work. The general systems based approach of defining a thermoacoustic system is outlined in The generic thermoacoustic model section, before treating in detail the two subsystems acoustics/flow and flame in The acoustics/flow subsystem and The flame subsystem sections, respectively. To simplify exposition, we exclusively deal with linear time-invariant (LTI) systems. An extension to the nonlinear regime is conceivable, but exceeds the scope of the present work.

The generic thermoacoustic model

As mentioned in the introduction, the thermoacoustic system is viewed as a combination of two subsystems in feedback: the acoustics/flow subsystem (index A) and the flame subsystem (index F). The dynamics of each subsystem is governed by a continuous state and a continuous output equation without feedthrough

$$\frac{\partial x_i}{\partial t} = \mathcal{A}_i\, x_i + \mathcal{B}_i\, u_i \tag{1a}$$

$$y_i = \mathcal{C}_i\, x_i \tag{1b}$$

The state vector of each subsystem $x_i(t)$ (where $i{=}A$ and $i = F$ for the subsystems acoustics/flow and flame, respectively) consists of N_i state functions defined for $t > 0$ on the system domains $\Omega_i \subset \mathbb{R}^3$ bounded by the system boundaries $\partial\Omega_i$, so $x_i : \mathbb{R}_0^+ \times \Omega_i \to \mathbb{R}^{N_i}$. The vectors $u_i(t)$ and $y_i(t)$ denote input and output to each of the subsystems, and are respectively defined on the input domains $\Omega_{u,i} \subset \mathbb{R}^\infty$ and system domains $\Omega_i \subset \mathbb{R}^3$. Thus, $u_i : \mathbb{R}_0^+ \times \Omega_{u,i} \to \mathbb{R}^{M_i}$ and $y_i : \mathbb{R}_0^+ \times \Omega_i \to \mathbb{R}^{P_i}$, with number of inputs and outputs, M_i and P_i, respectively. The operators $\mathcal{A}_i : \mathbb{R}^{N_i} \to \mathbb{R}^{N_i}$, $\mathcal{B}_i : \mathbb{R}^{M_i} \to \mathbb{R}^{N_i}$, and $\mathcal{C}_i : \mathbb{R}^{N_i} \to \mathbb{R}^{P_i}$ are continuous partial differential operators of state, input, and output, respectively.

The two subsystems acoustics/flow and flame are interconnected by coupling the respective inputs u_i and outputs y_i. That is, the output of the acoustics/flow subsystem is fed as input into the flame subsystem, and vice versa, $u_F = y_A = \mathcal{C}_A\, x_A$ and $u_A = y_F = \mathcal{C}_F\, x_F$. Stacking both individual state vectors accordingly, and combining the dynamics of the individual subsystems, we obtain the governing equations of the fully coupled thermoacoustic system defined on the system volume $\Omega \subset \mathbb{R}^3$

$$\frac{\partial x}{\partial t} = \mathcal{A}\, x + \mathcal{B}\, u \tag{2a}$$

$$y = \mathcal{C}\, x \tag{2b}$$

where

$$x = [x_A\ ,\ x_F]^T, \quad \text{and} \quad \mathcal{A} = \begin{bmatrix} \mathcal{A}_A & \mathcal{B}_A\mathcal{C}_F \\ \mathcal{B}_F\mathcal{C}_A & \mathcal{A}_F \end{bmatrix} \tag{3}$$

with state, input, and output operators, $\mathcal{A} : \mathbb{R}^N \to \mathbb{R}^N$, $\mathcal{B} : \mathbb{R}^M \to \mathbb{R}^N$ and $\mathcal{C} : \mathbb{R}^N \to \mathbb{R}^P$. The input u and output y govern the input and output to the *entire* thermoacoustic system. This includes the possibility of forcing any of the individual states of both subsystems, as well as defining the output as an arbitrary linear combination of any of the individual states of both subsystems. The number of state functions, inputs and outputs are given by N, M, and P, respectively. The full thermoacoustic model is complete and fully specified if and only if the continuous operators $\mathcal{A}$, $\mathcal{B}$ and $\mathcal{C}$ are defined. We call the set $(\mathcal{A}, \mathcal{B}, \mathcal{C})$ a continuous *model* that describes the dynamical behavior of the thermoacoustic system.

The dynamics of the continuous thermoacoustic model given in equation (2) is measurable by a scalar metric, which is defined as the L_2-norm of the output y. This so-called *output energy* $\mathcal{E}(t) : \mathbb{R}_0^+ \times \mathbb{R}^P \to \mathbb{R}_0^+$ thus corresponds to a weighted inner state product

$$\begin{aligned} \mathcal{E} &= \| y\|_2^2 = \int_\Omega y^T y\ \mathrm{d}\Omega \\ &= \int_\Omega x^T \mathcal{C}^T \mathcal{C}\, x\ \mathrm{d}\Omega = \int_\Omega x^T \mathcal{W} x\ \mathrm{d}\Omega \end{aligned} \tag{4}$$

with energy weighting operator $\mathcal{W} = \mathcal{C}^T\mathcal{C} : \mathbb{R}^N \to \mathbb{R}^N$. The term output energy does not necessarily allude to a physical energy measure with conservative properties, but merely originates from the fact that it is a square measure of the output y.

Upon discretization or modal expansion, the sets of partial differential state and output equation (2) reduce to ordinary differential equations (ODE)

$$\frac{\mathrm{d}\mathbf{x}}{\mathrm{d}t} = \mathbf{A}\,\mathbf{x} + \mathbf{B}\,\mathbf{u} \tag{5a}$$

$$\mathbf{y} = \mathbf{C}\,\mathbf{x} \tag{5b}$$

with discrete state, input, and output vectors $\mathbf{x} \in \mathbb{R}^N$, $\mathbf{u} \in \mathbb{R}^M$, $\mathbf{y} \in \mathbb{R}^P$, respectively, and state, input, and output matrices $\mathbf{A} \in \mathbb{R}^{N\times N}$, $\mathbf{B} \in \mathbb{R}^{N\times M}$, and $\mathbf{C} \in \mathbb{R}^{P\times N}$, respectively. M, N, and P represent the respective number of discrete inputs, states, and outputs. We call the set $(\mathbf{A}, \mathbf{B}, \mathbf{C})$ a discrete state space model (SSM) that describes the dynamical behavior of the thermoacoustic system. The analytical solution to the output $\mathbf{y}$ reads

$$\mathbf{y}(t) = \mathbf{C}\, e^{\mathbf{A}t}\, \mathbf{x}_0 + \int_{t_0}^{t} \mathbf{C}\, e^{\mathbf{A}(t-\tau)}\, \mathbf{B}\, \mathbf{u}(\tau)\mathrm{d}\tau \tag{6}$$

with initial condition $\mathbf{x}_0 = \mathbf{x}(t_0)$, and $t_0 = 0$ without loss of generality. The first and second terms constitute the free and forced response, respectively.

In analogy to the output energy $\mathcal{E}$ of the continuous model $(\mathcal{A}, \mathcal{B}, \mathcal{C})$, the dynamics of the discrete model $(\mathbf{A}, \mathbf{B}, \mathbf{C})$ is measurable by the scalar output energy $E(t) : \mathbb{R}_0^+ \times \mathbb{R}^P \to \mathbb{R}_0^+$

$$E = \|\mathbf{y}\|_2^2 = \mathbf{y}^T\mathbf{y} = \mathbf{x}^T\mathbf{C}^T\mathbf{C}\,\mathbf{x} = \mathbf{x}^T\mathbf{W}\,\mathbf{x} \tag{7}$$

with a symmetric energy weighting matrix $\mathbf{W} = \mathbf{C}^T\mathbf{C} \in \mathbb{R}^{N\times N}$. As for $\mathcal{E}$, E does not necessarily correspond to a physical energy with conservative properties unless $\mathbf{C}$ (or $\mathbf{W}$) is defined accordingly.

In the following two sections, we define the specific subsystems acoustics/flow and flame, which are substituted into the generic thermoacoustic model defined above to form the specific thermoacoustic model investigated in the present study.

The acoustics/flow subsystem

The thermoacoustic setup consists of a straight duct with length L_A and constant cross-sectional area A_A. The spatial domain of the duct is defined by the 1-D set $X = \{\xi\ :\ \xi \in [0, 1]\}$. A heat source is located at $\xi = \xi_F$, as depicted in Figure 2. The spatial extent of the flame is assumed to be much smaller than an acoustic wave length, so the flame is treated as acoustically compact. The mean pressure is assumed constant everywhere, because the Mach number is small. Both duct ends are treated as acoustically open, which corresponds to perfectly reflective ends with $p = 0$. The dissipative effects of heat and viscous diffusivity are modeled by negative semidefinite damping terms for velocity and pressure, ζ_v and ζ_p, respectively.

Assuming homentropic planar acoustic waves, the equations governing the acoustic velocity v and pressure p are given by the linearized Euler equations in one spatial dimension ξ[39,40,41]

$$\frac{\partial v}{\partial t} = -M\,\frac{\partial v}{\partial \xi} - \left(3\frac{\partial M}{\partial \xi} - \zeta_v\right) v - \frac{\partial p}{\partial \xi}, \tag{8a}$$

$$\frac{\partial p}{\partial t} = -\frac{\partial v}{\partial \xi} - \frac{1}{\beta}\frac{\partial \beta}{\partial \xi}\, v - M\,\frac{\partial p}{\partial \xi} - \left(2\gamma\frac{\partial M}{\partial \xi} - \zeta_p\right) p + K\,\dot{q}\,d \tag{8b}$$

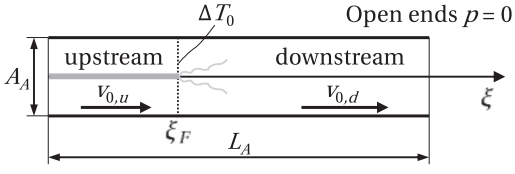

Figure 2. One-dimensional duct configuration with non-zero mean flow v_0 and non-zero mean temperature jump ΔT_0 resulting from the heat source located at ξ_F The open duct ends are acoustically fully reflective.

which have been non-dimensionalized by the reference scales

$$v_{\text{ref}} = c_0, \quad \xi_{\text{ref}} = L_A, \quad p_{\text{ref}} = \rho_0\, c_0^2, \quad \dot{q}_{\text{ref}} = \dot{q}_0,$$
$$t_{\text{ref}} = \frac{\xi_{\text{ref}}}{v_{\text{ref}}} = \frac{L_A}{c_0} = t_A, \quad \zeta_{\text{ref}} = \frac{1}{t_{\text{ref}}} = \frac{c_0}{L_A}, \quad d_{\text{ref}} = \frac{1}{L_A} \tag{9}$$

in order to bring pressure and velocity perturbations to the same order of magnitude. The steps of non-dimensionalization are presented in Appendix. 1.

The term $\beta = \beta(\xi)$ in equation (8(b)), which expresses the spatial profile of the speed of sound normalized by its mean value upstream of the heat source, is a function of the temperature profile along the duct,

$$\beta(\xi) = \frac{c_0(\xi)}{c_{0,u}} = 1 + \Delta_\beta \int_0^\xi \mathrm{d}(\tilde{\xi})\ \mathrm{d}\tilde{\xi} \tag{10}$$

with the 1-D spatial profile of heat addition d, the temperature incremental factor $\Delta_\beta = \sqrt{T_{0,d}/T_{0,u}} - 1$, and $T_{0,d}/T_{0,u}$ the ratio of mean temperatures down- (index d) and upstream (index u) of the heat source. Equivalently, $\Delta_\beta = c_{0,d}/c_{0,u} - 1$ is related to the ratio of speeds of sound. The Mach number is defined as $M = v_0/c_0$. As the bulk mean flow must obey continuity $\rho_0 v_0 = const.$, the local Mach number varies as $M_d = (\Delta_\beta + 1)\, M_u$, and thus

$$M(\xi) = \frac{v_0(\xi)}{c_0(\xi)} = M_u \left(1 + \Delta_\beta \int_0^\xi \mathrm{d}(\tilde{\xi})\ \mathrm{d}\tilde{\xi}\right) \tag{11}$$

Finally, the strength of the heat source is regulated by the scalar

$$K = K_0\,(\gamma - 1)\,\frac{\dot{q}_0}{\rho_0\, c_0^3\, A_A} \tag{12}$$

which weights the mean heat release rate per duct area against an equivalent acoustic power per unit area. The parameter K_0 has been introduced to adjust the strength of the fluctuating heat source.

In reality, the parameter $K_0 = 1$, such that mean flow, damping, the temperature jump and the strength of the heat source are not independent from each other. Whatever heat is produced by the heat source spreads by convection and molecular diffusion; if it is a reacting heat source, fresh combustibles are transported to the flame by the mean flow, and so on. However, the simple model given in terms of equation (8) contains M_u, Δ_β, K_0 and ζ_i as independent parameters. This provides a basis for investigating different effects separately: the effect of mean flow (controlled by M_u), the effect of a fluctuating heat source (controlled by Δ_β, K, and d), and the effect of damping terms (regulated by ζ_v, ζ_p). Unless otherwise mentioned, we use the default parameter values for the acoustics/flow subsystem as given in the first columns of Table 1 (with the damping values ζ_1 and ζ_2 as introduced in equation (48) below).

Table 1. Parameter values of the low-order thermoacoustic model as used in the present study: flame position ξ_F, damping coefficients ζ_1 and ζ_2, temperature incremental factor Δ_β, upstream Mach number M_u, Strouhal number Sr, equivalence ratio ϕ, flame angle α, ratio of convective to mean flow velocity μ, and the type of the laminar premixed flame.

	Acoustic			Mixed				Flame		
	ξ_F	ζ_1	ζ_2	Δ_β	M_u	Sr	ϕ	α	μ	Type
Default	0.2	–0.08	–0.025	1.25	0.005	1	0.85	23°	0.9	Wedge
Low damping	0.2	–0.01	–0.005	1.25	0.005	1	0.85	23°	0.9	Wedge

In the present study, the heat source is assumed acoustically compact. The heat is thus locally added to the flow field at the position of the compact heat source ξ_F, and the mean quantities remain constant upstream and downstream of the heat source, respectively. That is, the mean temperature T_0, density ρ_0 and speed of sound c_0 exhibit a jump at ξ_F. We therefore define the 1-D spatial profile d appearing in equations (10) and (11) as a Dirac measure δ_{ξ_F} for any subset $X_A \subseteq X$

$$d = \delta_{\xi_F}(X_A) = \begin{cases} 1 & \text{if } \xi_F \in X_A \\ 0 & \text{if } \xi_F \notin X_A \end{cases} \tag{13}$$

Consequently, the identity

$$\int_{X_A} \Phi(\tilde{\xi})\, \delta_{\xi_F}(\tilde{\xi})\ \mathrm{d}\tilde{\xi} = \begin{cases} \Phi(\xi_F) & \text{if } \xi_F \in X_A \\ 0 & \text{if } \xi_F \notin X_A \end{cases} \tag{14}$$

holds for any given function $\Phi(\xi)$.

With this definition for d, equations (10) and (11) become

$$\beta(\xi) = \begin{cases} 1 & \text{for } 0 \le \xi < \xi_F \\ 1 + \Delta_\beta & \text{for } \xi_F \le \xi \le 1, \end{cases}$$
$$M(\xi) = \begin{cases} M_u & \text{for } 0 \le \xi < \xi_F \\ M_u\,(1 + \Delta_\beta) & \text{for } \xi_F \le \xi \le 1 \end{cases}$$

and the terms $1/\beta\, \partial\beta/\partial\xi$ and $\partial M/\partial\xi$ in equation (8) read

$$\frac{1}{\beta}\frac{\partial\beta}{\partial\xi} = \begin{cases} \frac{\Delta_\beta}{1+\Delta_\beta} & \text{for } \xi = \xi_F \\ 0 & \text{for } 0 \le \xi < \xi_F \wedge \xi_F < \xi \le 1, \end{cases}$$
$$\frac{\partial M}{\partial\xi} = \begin{cases} M_u\, \Delta_\beta & \text{for } \xi = \xi_F \\ 0 & \text{for } 0 \le \xi < \xi_F \wedge \xi_F < \xi \le 1 \end{cases}$$

For non-compact heat sources, other spatial profiles of heat addition are conceivable (e.g. a Gaussian or a polynomial function).

Defining the states of the acoustics subsystem as the spatially distributed acoustic velocity $v(\xi)$ and pressure $p(\xi)$, the set of governing equations (8) constitutes the state equation of the acoustics/flow subsystem. Fluctuations in heat release rate $\dot{q}$ hence act as input to the acoustics/flow subsystem. We further define the output as the acoustic velocity fluctuations at the position of the heat source, $v_F \equiv v(\xi_F)$, which in turn are fed as input into the flame subsystem (see The flame subsystem section). The resulting continuous model $(\mathcal{A}_A, \mathcal{B}_A, \mathcal{C}_A)$ defined in equation (1) thus reads

$$\mathcal{A}_A = \begin{bmatrix} -M\,\dfrac{\partial}{\partial\xi} - \left(3\dfrac{\partial M}{\partial\xi} - \zeta_v\right) & -\dfrac{\partial}{\partial\xi} \\ -\dfrac{\partial}{\partial\xi} - \dfrac{1}{\beta}\dfrac{\partial\beta}{\partial\xi} & \begin{Bmatrix} -M\,\dfrac{\partial}{\partial\xi} \\ -\left(2\gamma\frac{\partial M}{\partial\xi} - \zeta_p\right) \end{Bmatrix} \end{bmatrix}$$
$$\mathcal{B}_A = \begin{bmatrix} 0 \\ K\,d \end{bmatrix}, \quad \mathcal{C}_A = [d \quad 0] \tag{15}$$

with states, input, and output

$$x_A = [\,v(\xi)\,,\; p(\xi)\,]^T, \quad u_A = \dot{q}, \quad y_A = v_F \tag{16}$$

The continuous model of the acoustics/flow subsystem is converted to the discrete model $(\mathbf{A}_A, \mathbf{B}_A, \mathbf{C}_A)$ using a MWR. In contrast to other numerical schemes such as finite differences, the MWR exhibits little spurious non-normality.[41] The details of the MWR and the associated damping model are specified in Appendix 2.

The flame subsystem

The heat sources present in thermoacoustic systems can be of many forms. The present study, however, exclusively deals with a premixed flame as heat source, from which the label *flame subsystem*. It is reasonable to assume that a premixed flame is primarily sensitive to velocity fluctuations, because its response to pressure fluctuations is marginal. We further assume the response of the premixed flame to be linear and time-invariant, such that its response behavior at any time $t > 0$ is fully characterized by its impulse response function $h(t) : \mathbb{R}^+ \to \mathbb{R}$.[42] Consequentially, the fluctuating heat release rate of the flame $\dot{q}$ can be modeled as a convolution of its impulse response (IR) function h and the lagged acoustic velocity fluctuations at the flame base v_F

$$\dot{q} = \int_0^{t_F} h(\tau)\, v_F(t-\tau)\; \mathrm{d}\tau = h * v_F \tag{17}$$

The upper integration limit t_F represents the finite settling time of the flame.

In the present study, the IR function h originates from the analytical solution of a laminar premixed wedge flame subject to convective velocity perturbations, where the flame is modeled in a level-set approach (G-Equation framework).[32,43–45] It has been reported that this low-order model is capable of reproducing fairly realistic flame behavior observed for laminar wedge flames in both the linear[46] and nonlinear regime.[47] However, in general, the formulation of $\dot{q}$ in equation (17) allows for any linear filter deduced from experiments or numerical simulations.[48,49] In the simplest case, $h(\tau) = n\,\delta(t-\tau_0)$ represents the well-known n-τ-model frequently used in the thermoacoustic community. The Laplace transform of h yields the flame transfer function in complex-valued frequency space.[32,50]

The IR function h of the laminar premixed wedge flame used in the present study is derived and discussed in detail in literatures.[32,41] In dimensional form, its analytical expression[41] reads

$$h(t) = \frac{\dot{q}_0}{2R_F^2}\sin^2(2\alpha)\begin{cases} \dfrac{-1}{\cos^2\alpha}\,w\,t & 0 \le t \le \tau_c \\ \dfrac{1}{1-\Pi}\,v_0\,t & \tau_c < t \le \tau_r \\ 0 & \text{otherwise} \end{cases} \tag{18}$$

where $\dot{q}_0$, R_F and α denote the mean heat release rate, the flame radius, and the flame angle, respectively. The convective forcing and mean flow velocities are given by w and v_0, respectively. In the present model, the settling time of the flame t_F is given by the characteristic time scale of restoration $\tau_r = 2\,R_F/(v_0\,\sin(2\alpha))$. $\tau_c = R_F/(w\,\tan\alpha)$ stands for the characteristic time scale of convective forcing, and the ratio of time scales Π is defined as

$$\Pi = \frac{\tau_c}{\tau_r} = \frac{\cos^2\alpha}{\mu} \tag{19}$$

with ratio of convective to mean flow velocity $\mu = w/v_0$. Assuming a fixed mean heat release rate $\dot{q}_0$, flame radius R_F and mean flow velocity v_0, the free parameters of the present flame model thus consist of the flame angle α and the convective forcing velocity w, which in turn is controlled by μ. The shape of the IR function is plotted in Figure 3 for three values of Π,

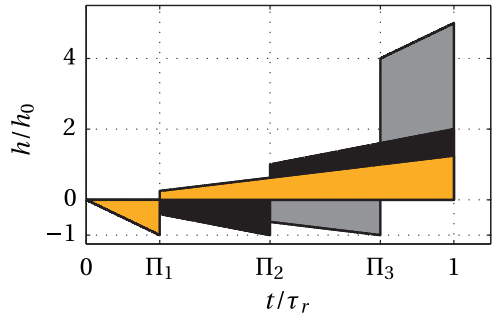

Figure 3. IR function h of the laminar premixed wedge flame used in the present study normalized by $h_0 = \dot{q}_0 \sin(2\alpha)/R_F$ for different ratios of time scales Π.

indicative of different combinations of α and μ. It is visible that the portion of the flame response for $t > \tau_c$ becomes more pronounced for increasing Π.

Equation (17) describes the output equation of the flame subsystem. Fluctuations in heat release rate $\dot{q}$ thus represent the output of the flame subsystem, which is fed as input into the acoustics/flow subsystem. In order to represent the flame subsystem in input–state–output form according to equation (1), it is necessary to find an evolution equation which represents the dynamics of the lagged acoustic velocity fluctuations. The latter state equation takes the form of an advection equation, where the current input $v_F(t)$ is propagated in history τ at a rate of $1/\mathrm{Sr}$

$$\frac{\partial v_F(t-\tau)}{\partial t} = -\frac{1}{\mathrm{Sr}} \frac{\partial v_F(t-\tau)}{\partial \tau} + v_F(t) \tag{20}$$

The Strouhal number $\mathrm{Sr} = t_F/t_A$ represents the ratio of the characteristic time scales of flame to acoustics, i.e. a ratio of the time scales of convective transport and wave propagation. The advection velocity in equation (20) scales inversely with Sr to convert the non-dimensional time of flame dynamics into the non-dimensional acoustic time scale. For common applications, such as heated wires or premixed flames, Sr is of the order of $10^0 \ldots 10^1$.[51]

In addition to Sr, the flame model is characterized by the flame angle α, the equivalence ratio ϕ, and the ratio of convective to mean flow velocity μ.[41,52] The convective velocity represents the rate at which perturbations are advected through the flame front. Unless otherwise mentioned, we use the default parameter values for the flame subsystem as given in the last columns of Table 1.

Converting the equations governing the dynamics of the states $v_F(t-\tau)$ and the output $\dot{q}$ to input–state–output form, the resulting continuous model $(\mathcal{A}_F, \mathcal{B}_F, \mathcal{C}_F)$ defined in equation (1) thus reads

$$\mathcal{A}_F = -\frac{1}{\mathrm{Sr}} \frac{\partial}{\partial \tau}, \quad \mathcal{B}_F = \mathcal{I}, \quad \mathcal{C}_F = h* \tag{21}$$

with states, input, and outputs

$$x_F = v_F(t-\tau), \quad u_F = v_F, \quad y_F = \dot{q} \tag{22}$$

The continuous model is converted to the discrete model $(\mathbf{A}_F, \mathbf{B}_F, \mathbf{C}_F)$ by uniform discretization of x_F in τ-direction

$$\mathbf{x}_F = [\, v_F(t-\Delta\tau),\, v_F(t-2\Delta\tau),\, \cdots,\, v_F(t-N_F\Delta\tau)\,]^T, \quad N_F\Delta\tau = t_F \tag{23}$$

The partial differential in the state equation (20) is approximated by finite elements with a zero gradient outflow condition, and the convolution integral in the output equation (17) is solved by trapezoidal summation. The set of discrete operators $(\mathbf{A}_F, \mathbf{B}_F, \mathbf{C}_F)$ is explicitly given in Appendix 3. Since the flame subsystem is SISO, the continuous and discrete input and output are the same, $\mathbf{u}_F = u_F = v_F$, and $\mathbf{y}_F = y_F = \dot{q}$.

Discussion of output energy

This section is dedicated to the first objective of the present paper. We intend to demonstrate that the choice of output energy merely defines the perspective from which the results should be interpreted, and therefore should be a matter of choice. This topic is addressed in The output defines the perspective section, before defining the output of the thermoacoustic model used in the present study in The output of the low-order thermoacoustic model section.

The output defines the perspective

The output equation of the continuous model defined in equation (2) shows that an output is a function of states $y = \mathcal{C}\,x$. The output is therefore entirely defined by the output operator $\mathcal{C}$, which weights the impact of the individual states onto the output. It is further defined in equation (4) that the energy $\mathcal{E}$ of the continuous model corresponds to the L_2-norm of the output y. In the absence of forcing, that is, for the autonomous continuous model $(\mathcal{A}, \mathcal{C})$, the temporal variation of the output energy $\mathcal{E}$ can be expressed by a classical energy balance

$$\frac{\partial}{\partial t}\mathcal{E} = \left(\int_\Omega \nabla \cdot f + s \; \mathrm{d}\Omega \right) = \int_{\partial\Omega} f \cdot \mathbf{n} \; \mathrm{d}\Omega + S \tag{24}$$

with flux and source terms f and s, respectively, and vector $\mathbf{n}$ normal to the boundary. The supply rate to the evolution of output energy $\mathcal{E}$ (i.e. the right-hand

side of equation (24)) consists of a net flux $\int_{\partial\Omega} f \cdot \mathbf{n}\, \mathrm{d}\Omega$ over the domain boundaries $\partial\Omega$ and a net source S within the domain volume Ω. The energy $\mathcal{E}$ may thus increase and decrease through a positive and negative supply rate, respectively.

The above supply rate governing $\partial\mathcal{E}/\partial t$ unambiguously results from the definition of the autonomous model $(\mathcal{A}, \mathcal{C})$, as this fixes how much energy is produced or dissipated. The flux and source terms contained in the supply rate can be derived analytically if the continuous model is available analytically. Depending on the definition of the output given by the output operator $\mathcal{C}$, the dynamics given by the state operator $\mathcal{A}$ shows up in equation (24) either as part of the output energy $\mathcal{E}$, or as flux or source terms f and S, respectively.

Since $\mathcal{C}$ does not affect the dynamics as such, which is entirely given by $\mathcal{A}$, the definition of $\mathcal{C}$ is a matter of choice. The output thus merely defines the perspective that the investigator chooses to have on the problem, and how the dynamics evolves from the chosen viewpoint. As stated in the introductory the Motivation and scope section, the question of appropriate energy norm should thus be restated as a question of appropriate *perspective* (''you get what you ask for'').

The choice of output may be motivated by physical or mathematical arguments, practical reasons such as diagnostic capabilities in experiments, modeling constraints or simply by personal preference. As examples for these categories, the output energy may be chosen to correspond to a physical energy or to a Lyapunov function; it may be chosen such that it represents a quantity that is accessible in an experiment; it may be chosen to penalize an unwanted effect that results from a given numerical scheme; or it may be chosen to represent a measure that can be used to support or to reject a certain hypothesis. However, as the output defines the perspective in which the results can be interpreted, some outputs may be more apt to show a given circumstance than others. That is, some outputs may suggest a misleading conclusion or an incomplete picture, which other outputs may not. We will elaborate on these points in the following using two examples from thermoacoustics.

The first example is taken from the literature, where Wieczorek et al.[17] analyze the non-normal transient growth of a non-isentropic thermoacoustic system with a non-zero steady heat source (i.e. $\dot{q} = 0$, but $\dot{q}_0 \neq 0$). The system is described by two autonomous models that only differ in the definition of output, $(\mathcal{A}, \mathcal{C}_1)$ and $(\mathcal{A}, \mathcal{C}_2)$. The system dynamics contained in $\mathcal{A}$ is given by the dimensional form of the linearized Euler equation (8), plus an evolution equation for entropy fluctuations σ (the entire set of governing equations treated by Wieczorek et al. is given in equation (2.5) to (2.7) in Nicoud and Wieczorek[53]; for further details, see Wieczorek et al.[17]). The output operator of the first model $\mathcal{C}_1$ is chosen such that the output energy $\mathcal{E}_1$ corresponds to the acoustic energy as derived by Cantrell and Hart,[33] which measures the kinetic and potential perturbation energy of the acoustic field with mean flow

$$\mathcal{E}_1 = \frac{1}{2}\int_\Omega \left[\rho_0 v^2 + 2\rho v_0 \cdot v + \frac{p^2}{\rho_0 c_0^2}\right] \mathrm{d}\Omega \qquad (25)$$

The output operator of the second model $\mathcal{C}_2$ is chosen such that $\mathcal{E}_2$ additionally takes into account fluctuations in entropy σ

$$\mathcal{E}_2 = \mathcal{E}_1 + \frac{1}{2}\int_\Omega \frac{\rho_0 T_0 \sigma^2}{c_p}\, \mathrm{d}\Omega \qquad (26)$$

This perturbation energy was first rigorously derived by Myers.[38] Wieczorek et al. report a significant difference in the upper bound of possible energy amplification between the models, $G_{\max,1} = \mathcal{O}(10^3)$ and $G_{\max,2} = \mathcal{O}(10^0)$ (see Figure 4). This difference is explained by the fact that the optimal initial state can contain non-zero entries in σ, which are not accounted for in the acoustic energy. The output energy of the first model $\mathcal{E}_1$ subsequently increases significantly when these entropy perturbations are converted to acoustics.

This finding can also be explained by comparing the flux and source terms of both models, which are responsible for driving or dissipating the respective output energies $\mathcal{E}_1(t)$ and $\mathcal{E}_2(t)$ over time. As introduced in the discussion following equation (24), the temporal evolution of $\mathcal{E}$ is governed by the flux and source terms resulting from the model definitions. That is, depending on the definition of output energy, the dynamics of the model is balanced as part of the output energy, or alternatively as flux or source terms. For the case

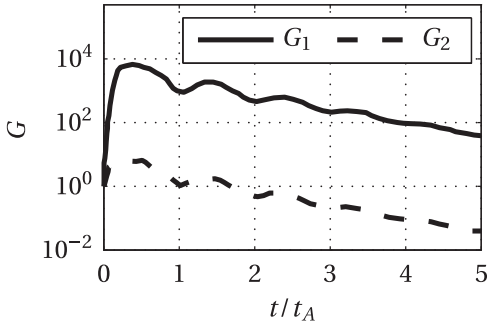

Figure 4. $G(t)$ of $(\mathcal{A},\mathcal{C}_1)$ (—) and of $(\mathcal{A},\mathcal{C}_2)$ (—). $G_{\max,1} = 6.7 \times 10^3$ and $G_{\max,2} = 6.5$. Figure redrawn from Figure 4(a) in Wieczorek et al.[17]

of Wieczorek et al., the differences in flux and source terms, which lead to the difference in temporal evolution of energies $\partial\mathcal{E}_1/\partial t - \partial\mathcal{E}_2/\partial t$, are derived analytically as

$$f_1 = f_2 + \frac{\rho_0 v_0}{2}\,\sigma_0\,\frac{\sigma_0 T_0}{c_p}\left(\frac{\sigma}{\sigma_0}\right)^2 \tag{27a}$$

$$S_1 = S_2 + \int_{L_A} \rho_0 v_0\,\frac{\sigma_0 T_0}{c_p}\left(\frac{\sigma}{\sigma_0}\right)\left(\frac{v}{v_0}\right)\frac{\partial\sigma_0}{\partial\xi}\;\mathrm{d}\xi \tag{27b}$$

The additional flux term in equation (27(a)) is strictly positive and expresses the fact that regions of fluctuating entropy (the so-called hot spots) exit the domain downstream. This process is not contained in the definition of $\mathcal{E}_1$ and thus shows up as flux term (unphysically) generating $\mathcal{E}_1$ at the downstream boundary. The entropy perturbations are created by the interaction of the acoustic field with a mean entropy gradient, as indicated by the additional source term in equation (27(b)). As before, $\mathcal{E}_1$ does not contain a measure for this transfer of kinetic to internal energy. This leads to an additional (unphysical) source term.

The order of magnitude of the additional flux and source terms can be estimated using the parameters given in Wieczorek et al.[17] With $\rho_0 v_0 \approx \mathcal{O}(10^1)$, $\sigma_0 T_0/c_p \approx \mathcal{O}(10^3)$, $\sigma_0 \approx \mathcal{O}(10^3)$ downstream of the heat source, $\partial\sigma_0 \approx \Delta\sigma_0 = c_v \ln(\Delta T_0) \approx \mathcal{O}(10^3)$, $v/v_0 \approx \mathcal{O}(10^{-2})$ and $\sigma/\sigma_0 \approx \mathcal{O}(10^{-2})$, both additional terms are of the order of 10^3, which corresponds nicely to the observed difference in $G_{\max}$. The difference in non-normal transient growth can hence be fully explained by the difference in the order of magnitude of f and S driving the energies of the models $(\mathcal{A}, \mathcal{C}_1)$ and $(\mathcal{A}, \mathcal{C}_2)$.

This example shows that the system dynamics may exhibit itself very differently subject to a different output, which, as seen above, results mathematically from weighting the states of the model differently in the definition of output. A different definition of output amounts to a change in perspective. For the above example, choosing $\mathcal{E}_2$ seems straightforward from a physical point of view. However, the definition of $\mathcal{E}_1$ and the corresponding change of perspective do not alter the dynamics as such (which are the same for both models), but merely requires the result to be interpreted accordingly. Choosing $\mathcal{E}_1$ will lead to the same conclusion if the altered perspective is taken into account in the interpretation of results.

Consider as a second example the thermoacoustic model introduced in The low-order thermoacoustic model section with fully reflective ends and a non-zero temperature jump at the center of the duct. We exclude fluctuations in heat release rate (i.e. we consider a flame with $K=0$), and neglect damping and mean flow (i.e. $\zeta_i = 0$ and $M_u = 0$). Since the state vector of the corresponding model reads $x = [v(\xi), p(\xi)]^T$ (see also equation (16)), it is straightforward to use the acoustic energy as output. This choice fixes $\mathcal{C}$ and closes the model $(\mathcal{A}, \mathcal{C})$. For this academic test case, physical arguments suggest that the fluctuating energy content of the system remains constant over time, as there are no physical sources or sinks of energy. However, with the choice of $\mathcal{C}$, the temporal evolution of energy is derived analytically as

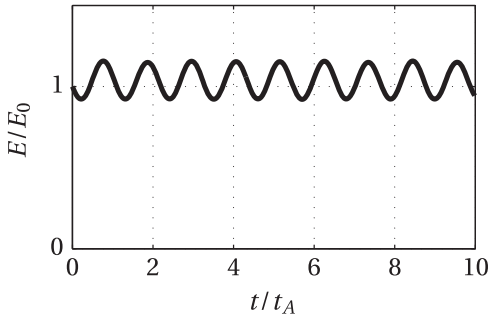

Figure 5. Time trace of output energy of the autonomous thermoacoustic model defined in The low-order thermoacoustic model section without damping and E representing acoustic energy E_A. Other parameters: $\xi_F = 0.2$, $M_u = 0$, $\Delta_\beta = 1.25$, $K = 0$.

$$\frac{\partial\mathcal{E}}{\partial t} = -v\,p\,\frac{1}{\beta}\frac{\partial\beta}{\partial\xi} \tag{28}$$

That is, the analysis identifies a source term in the region of the non-zero temperature gradient. The acoustic energy thus does not remain constant over time, which is visible from Figure 5. The output energy E of the corresponding discrete model oscillates around the initial value E_0.

This seemingly unphysical behavior with spurious energy growth and decay can be explained as follows. The heat source defines a flame at rest located at $\xi = \xi_F$. The flame is thus not able to move in response to an acoustic wave. Instead, a local increase in velocity leads to a larger volume of fresh gas being pushed into and consumed by the flame, and thus to more heat produced, because the downstream temperature is assumed constant. A local decrease in velocity due to $v < 0$ causes the opposite effect. We are thus left with the relation $\dot{q} \propto v$, which substituted into equation (28) yields a source term analog to the classical Rayleigh source term $\partial\mathcal{E}/\partial t \propto \dot{q}\,p_F$. The phenomenon of a flame at rest producing fluctuations in energy is referred to as "the classical paradox of thermoacoustics" by Bauerheim et al.[54] and is also explained by Strobio Chen et al.[55]

The above described mechanism of creating fluctuations in heat release rate is fundamentally different from the fluctuations in heat release rate resulting from an active flame as described in The flame subsystem

section (these fluctuations are excluded in the present example by definition). The active flame mechanism stems from the convectively driven response of premixed flames to acoustic perturbations, which are transformed to flame wrinkles at the flame base and advect along the flame with the mean flow. In contrast, the above mechanism with a flame at rest happens at an acoustic time scale. It results from simplistic modeling assumptions, because the model does not allow for movement of the center of heat release. The identified source term in equation (28) is thus physical, but, strictly speaking, the assumption as such of a flame at rest is not (although it is widespread in thermoacoustics). Both mechanisms have in common that they alter the acoustic energy via the Rayleigh and a Rayleigh-like source term, which only differ in the pre-factors K and $-1/\beta\,\partial\beta/\partial\xi$, respectively.

For this second example, the adopted perspective prescribed by the choice of output highlights the implicit assumptions and limitations of the model. A different output may have accounted for the inability of the heat source to move with flow perturbations, and yielded results that better match physical intuition (e.g. constant energy over time). However, this argument does not render one or another choice of output more or less appropriate.

The output of the low-order thermoacoustic model

Since the output energy is a matter of choice, we decide to close the thermoacoustic model introduced in The low-order thermoacoustic model section by using the acoustic energy as energy metric. Upon non-dimensionalization of equation (25) with the reference scales given in equation (9), the resulting output operator reads

$$\mathcal{C} = \frac{\sqrt{2}}{2}\begin{bmatrix} 1 & M & 0 \\ 0 & \sqrt{1-M^2} & 0 \end{bmatrix} \tag{29}$$

The corresponding output matrix $\mathbf{C}$ of the discrete model is given in Appendix. 3.

With the above choice of output energy, the flux and net source terms of the autonomous continuous thermoacoustic model $(\mathcal{A},\mathcal{C})$ due to which $\mathcal{E}$ varies in time are derived analytically as

$$f = -(M\,v^2 + (1+M^2)\,v\,p + M\,p^2) \tag{30(a)}$$

$$S = \underbrace{K\dot{q}\int_{L_A}[p + M\,v]\,d\;\mathrm{d}\xi}_{\text{(extended) Rayleigh source term}}$$

$$\underbrace{-\int_{L_A}\Bigg[\underbrace{\frac{\partial M}{\partial\xi}\,[4\,v^2 + M\,(3+\gamma)\,v\,p + 2\,\gamma\,p^2]}_{\text{source term related to gradients in mean flow}} + \underbrace{\frac{1}{\beta}\frac{\partial\beta}{\partial\xi}\,p\,v}_{\text{source term related to gradients in temperature}}\Bigg]\,\mathrm{d}\xi}$$

$$\underbrace{+\int_{L_A}[\zeta_v\,v^2 + M\,(\zeta_v+\zeta_p)\,v\,p + \zeta_p\,p^2]\,\mathrm{d}\xi}_{\text{damping term}} \tag{30(b)}$$

In the absence of mean flow, the flux term f reduces to the well-known acoustic flux $(v\,p)$ over the boundaries. However, in the present model, $p=0$ at the boundaries, so $f=-M\,v^2$. $\mathcal{E}$ thus increases (decreases) if a higher (lower) convective flux $M\,v^2$ enters the domain upstream than leaves the domain downstream.

The source term S given in equation (30(b)) consists of a term resulting from the interaction of the fluctuating heat source with the acoustic field (the first line of equation (30(b))), a source term related to the gradients in mean flow and temperature, $\partial M/\partial\xi$ and $\partial\beta/\partial\xi$, respectively (the second line of equation (30b)), and a damping term (the third line of equation (30(b))). For small mean flow (i.e. $M_u \ll 1$), the source terms in equation (30(b)) that depend on M and $\partial M/\partial\xi$ are negligible in magnitude. The main sources to $\mathcal{E}$ are thus the classical Rayleigh term $K\dot{q}\int_{L_A} p\,d\;\mathrm{d}\xi$, the Rayleigh-like source term due to the fixed flame assumption (see the last term in the second line of equation (30(b))), and two strictly dissipative damping terms (see the first and last terms in third line of equation (30(b))). As discussed in The output defines the perspective section, the Rayleigh-like source term results from the assumption of a flame at rest, which is inherent to the model. We therefore refer to this source term as *inherent source term* in the remainder of the present work.

Since the net flux and source terms are not strictly dissipative, it obviously follows that the thermoacoustic model $(\mathcal{A},\mathcal{C})$ admits transient growth. The main sources to $\mathcal{E}$ are the Rayleigh source term and the Rayleigh-like inherent source term, which scale with the strength of the heat source and the mean temperature jump, respectively. We therefore expect the strength of the heat source regulated by K and the magnitude of the temperature jump regulated by the temperature incremental factor Δ_β to dominate transient energy growth. This matter will be discussed in the Parameters influencing transient growth section.

As is visible from equation (29), the output energy $\mathcal{E}$ only includes states from the acoustics/flow subsystem and not from the flame subsystem. The acoustic energy thus describes a semi-norm. Investigating non-normal transient growth subject to semi-norms has so far only

been addressed by Foures et al.[34] in the context of variational methods, and recently also by Magri.[35] In the following section, we propose an approach to do so using SVD. This will allow us to investigate the basic mechanisms and dynamics of non-normal transient growth around a stable fix point in thermoacoustics in the Analysis of non-normal transient growth around a stable fix point section.

Optimization of output energy using SVD

This section deals with the theory to compute the maximization of output energy E associated to the discrete model $(\mathbf{A}, \mathbf{B}, \mathbf{C})$ introduced in The low-order thermoacoustic model section. Provided that the system is asymptotically stable, we define the *relative* amplification of output energy of an autonomous model (i.e. $\mathbf{u} = 0$) as

$$\mathcal{G}(t, \mathbf{x}_0) = \frac{E(t)}{E_0} = \frac{\|\mathbf{C}\, \exp(\mathbf{A}t)\, \mathbf{x}_0\|_2^2}{\|\mathbf{C}\, \mathbf{x}_0\|_2^2} \tag{31}$$

The output energy over time is thus measured with respect to the initial level of output energy at $t = 0$. To study non-normal transient growth, we are interested in finding the maximum $\mathcal{G}$ for all possible initial conditions $\mathbf{x}_0$. Applying such an optimization to equation (31) is mathematically sound if $\mathbf{C}$ is invertible. In this case, E defines a full norm of which the nullspace (kernel) is the trivial nullvector.[34] However, if $\mathbf{C}$ is singular, E does not include contributions from all states (of all subsystems). It thus defines a semi-norm, of which the kernel extends beyond the trivial nullvector. The optimization problem leading to the maximum of $\mathcal{G}$ is ill-posed if this nullspace is unbounded.[34] In this case, $\mathcal{G}$ can become unlimited because the contributions from those states (of those subsystems) that are not mirrored in E are not constrained in magnitude within the optimization.

In order to deal with a well-posed optimization problem, it needs to be ensured that the optimization procedure leading to the maximum output energy is performed with respect to a full norm. To this end, we define the *total state energy*

$$E_N(t) = \mathbf{x}^T \mathbf{W}_N\, \mathbf{x} = \|\mathbf{C}_N\, \mathbf{x}\|_2^2 = \|\mathbf{y}_N\|_2^2 \tag{32}$$

with the total state energy weighting matrix $\mathbf{W}_N \in \mathbb{R}^{N \times N}$, the total state output matrix $\mathbf{C}_N \in \mathbb{R}^{N \times N}$ and the total state output vector $\mathbf{y}_N \in \mathbb{R}^N$. The total state energy weighting matrix $\mathbf{W}_N$ is purposefully defined as a positive definite matrix, which is thus also non-singular. The latter is achieved by including identity matrices $\mathbf{I}$ of appropriate sizes in the nullspaces of the output energy weighting matrix $\mathbf{W}$ (if any). These nullspaces can be found by diagonalization of $\mathbf{W}$. The total state output matrix $\mathbf{C}_N$ is subsequently computed as the Cholesky decomposition of $\mathbf{W}_N$, and is therefore invertible (regular) by definition. By construction, the total state energy E_N is thus a full norm.

It is then possible to define the optimization problem leading to the maximum *normalized* output energy amplification as

$$\begin{aligned} G(t) &= \max_{\mathbf{y}_{N,0}} \frac{E(t)}{E_{N,0}} = \max_{\mathbf{y}_{N,0}} \frac{\|\mathbf{C}\, \exp(\mathbf{A}t)\, \mathbf{x}_0\|_2^2}{\|\mathbf{y}_{N,0}\|_2^2} \\ &= \max_{\mathbf{y}_{N,0}} \frac{\|\mathbf{C}\, \exp(\mathbf{A}t) \mathbf{C}_N^{-1}\|_2^2 \cdot \|\mathbf{y}_{N,0}\|_2^2}{\|\mathbf{y}_{N,0}\|_2^2} \\ &= \|\mathbf{C}\, \exp(\mathbf{A}t)\, \mathbf{C}_N^{-1}\|_2^2 \end{aligned} \tag{33}$$

where the last equality is obtained at optimality $\mathbf{y}_{N,0}^* = (\mathbf{C}_N\, \mathbf{x}_0)^*$ as a consequence of the definition of the L_2 matrix norm. As defined earlier, the total state output matrix $\mathbf{C}_N$ is a fixed regular matrix describing a bijective linear map. It is therefore not altered in the optimization problem leading to optimality, but merely weights the initial condition $\mathbf{x}_0$ over which the maximization in equation (33) is performed. The optimal initial condition is thus found by $\mathbf{x}_0^* = \mathbf{C}_N^{-1}\, \mathbf{y}_{N,0}^*$.

In contrast to the relative amplification of output energy $\mathcal{G}$, the maximum normalized amplification of output energy G is a measure of the output energy over time with respect to the initial level of total state energy E_N defined in equation (32). If $\mathbf{C}$ is invertible (and thus $\mathbf{W}$ does not contain any nullspaces), the total state energy equals the output energy, $E_N = E$, and thus $G = \max_{\mathbf{y}_0} \mathcal{G}$. Otherwise, E_N corresponds to a generic energy norm which is not necessarily a (physically) meaningful energy metric.

The difference between total state and output energy is expressed by the *kernel energy*

$$E^\dagger(t) = E_N(t) - E(t) = \mathbf{x}^T\, \mathbf{W}^\dagger\, \mathbf{x} \tag{34}$$

with kernel energy weighting matrix $\mathbf{W}^\dagger = \mathbf{W}_N - \mathbf{W}$. Following Foures et al.,[34] we define the ratio of kernel to output energy

$$\kappa(t) = \frac{E^\dagger(t)}{E(t)}, \quad 0 \leq \kappa \leq \infty \tag{35}$$

If the output energy E defines a semi-norm, $E^\dagger > 0$, and thus $\kappa > 0$. For $\kappa = 0\ \forall t$, the total state energy E_N and the output energy E coincide, and E defines a full norm. The ratio of kernel to output energy κ is not an absolute measure, as it depends on the definition of the total state energy weighting matrix $\mathbf{W}_N$. The exact

numeric values of κ are therefore of limited interest. However, κ serves as indication of how much energy is contained in the states (of those subsystems) that are not reflected in the output energy E.

The maximum possible (i.e. optimal) amplification of normalized output energy $G_{\max} = \max_t G(t)$ occurs at $t = t^*$, which is the time at optimality. Transient growth is possible if $G_{\max} > 1$. The optimal initial condition $\mathbf{x}_0^*$ (OIC) can be found from the singular value decomposition (SVD) of $\mathbf{C}\exp(\mathbf{A}t^*)\mathbf{C}_N^{-1} = \mathbf{D}\mathbf{S}\mathbf{P}^H$. $\mathbf{D} \in \mathbb{R}^{P\times P}$ and $\mathbf{P} \in \mathbb{R}^{N\times N}$ are unitary matrices of left- and right-singular vectors, respectively, and $\mathbf{S} \in \mathbb{R}^{P\times N}$ represents a diagonal matrix of singular values. The OIC $\mathbf{x}_0^*$ is the first right-singular vector multiplied by $\mathbf{C}_N^{-1}$ (see the discussion following equation (33)), which signifies the most amplified mode at $t = t^*$ by the action of $\mathbf{C}\exp(\mathbf{A}t)\mathbf{C}_N^{-1}$. The total state output vector at optimality $\mathbf{y}_N^*$ is given by the first left-singular vector. The optimal normalized energy growth $G_{\max}$ corresponds to the square of the first singular value on the diagonal of $\mathbf{S}$. The short-term dynamics of the output energy is thus not governed by the eigenvalues of $\mathbf{A}$, but by the singular values of $\mathbf{C}\exp(\mathbf{A}t)\mathbf{C}_N^{-1}$.[6]

Using SVD, the procedure to find the OIC is computationally simple and fast. However, if the output energy E defines a semi-norm, the resulting optimal normalized energy amplification given by $G_{\max}$ may not correspond to the maximum possible relative amplification of output energy $\mathcal{G}_{\max}$. This is because the optimization leading to $G_{\max}$ yields an optimal initial ratio of kernel to output energy κ_0^*, for which the *normalized* output energy is maximized. However, the optimization is not performed with respect to the optimal κ_0^* that would maximize the *relative* amplification of output energy $\mathcal{G}$. As highlighted in Foures et al.,[34] this "true" maximization of relative amplification of output energy requires κ to be taken into account as additional optimization parameter. This can only be done using variational methods, such as constrained optimization with Lagrangian multipliers (Lagrangian optimization). Variational methods are very flexible and powerful (for example, one can optimize for an infinite number of constraints or cost functions), at the cost of increased complexity and effort in computation and implementation. A comprehensive review on optimization and control for flow systems is given by Kim and Bewley.[56]

In the following, we propose an approach to avoid the above-mentioned issues related to semi-norm optimization while still resorting to SVD. To this aim, it is necessary to extend the above concept of energy maximization to include forcing. In analogy to the relative amplification of output energy of an autonomous model $\mathcal{G}$, and using equation (6), we define the *relative* amplification of output energy of a forced model as

$$\mathcal{H}(t,\mathbf{x}_0,\mathbf{u}) = \frac{E(t)}{E_0} = \frac{\|\mathbf{C}\left(\exp(\mathbf{A}t)\,\mathbf{x}_0 + \int_0^t \exp(\mathbf{A}(t-\tau))\,\mathbf{B}\,\mathbf{u}\;\mathrm{d}\tau\right)\|_2^2}{\|\mathbf{C}\left(\mathbf{x}_0 + \int_0^t \mathbf{u}\;\mathrm{d}\tau\right)\|_2^2} \tag{36}$$

The definition of $\mathcal{H}$ represents a maximization problem that includes a penalization of the energy needed to produce the forcing action. As for $\mathcal{G}$, the maximization problem to find the maximum $\mathcal{H}$ is ill-posed if $\mathbf{C}$ is singular. We therefore define the maximum *normalized* output energy amplification of a forced model as

$$H(t) = \max_{\mathbf{y}_{N,0}} \frac{E(t)}{E_{N,0}} = \max_{\mathbf{y}_{N,0}} \frac{1}{\|\mathbf{y}_{N,0}\|_2^2} \times \|\mathbf{C}\left(\exp(\mathbf{A}t)\,\mathbf{x}_0 + \int_0^t \exp(\mathbf{A}(t-\tau))\,\mathbf{B}\,\mathbf{u}\;\mathrm{d}\tau\right)\|_2^2 \tag{37}$$

where $\mathbf{y}_{N,0} = \mathbf{C}_N(\mathbf{x}_0 + \int_0^t \exp(\mathbf{A}(t-\tau))\,\mathbf{u}\;\mathrm{d}\tau)$. Depending on the applied input $\mathbf{u}$, the solution of equation (37) may present a significant challenge.

An autonomous system can be represented as a forced system that is initially at rest and forced impulsively at $t = 0$ (i.e., $\mathbf{x}_0 = 0$ and $\mathbf{u} = \mathbf{u}_0\,\delta(t)$). The role of the initial condition $\mathbf{x}(0) = \mathbf{x}_0$ is then taken by $\mathbf{x}(0) = \mathbf{B}\,\mathbf{u}_0$, with input matrix $\mathbf{B}$ as introduced in The generic thermoacoustic model section. We define $\mathbf{B} \in \mathbb{R}^{N\times N}$ as diagonal matrix with $\|\mathbf{B}\|_2 = 1$, such that it is ensured that $\mathbf{x}(0)$ is representable, i.e. that $\mathbf{x}(0) \in \mathrm{span}(\mathbf{B})$. Substituting $\mathbf{x}_0 = 0$ and $\mathbf{u} = \mathbf{u}_0\,\delta(t)$ in equation (37), the initial total output vector becomes $\mathbf{y}_{N,0} = \mathbf{C}_N\,\mathbf{u}_0$, and equation (37) reduces to

$$\begin{aligned} H(t) &= \max_{\mathbf{y}_{N,0}} \frac{E(t)}{E_{N,0}} = \max_{\mathbf{y}_{N,0}} \frac{\|\mathbf{C}\,\exp(\mathbf{A}t)\,\mathbf{B}\,\mathbf{u}_0\|_2^2}{\|\mathbf{y}_{N,0}\|_2^2} \\ &= \max_{\mathbf{y}_{N,0}} \frac{\|\mathbf{C}\,\exp(\mathbf{A}t)\,\mathbf{B}\,\mathbf{C}_N^{-1}\|_2^2 \cdot \|\mathbf{y}_{N,0}\|_2^2}{\|\mathbf{y}_{N,0}\|_2^2} \\ &= \|\mathbf{C}\,\exp(\mathbf{A}t)\,\mathbf{B}\,\mathbf{C}_N^{-1}\|_2^2 \end{aligned} \tag{38}$$

where the last equality is obtained at optimality $\mathbf{y}_{N,0}^* = (\mathbf{C}_N\,\mathbf{u}_0)^*$ as a consequence of the definition of the L_2 matrix norm. As for the autonomous case, the total state output matrix $\mathbf{C}_N$ is not altered in the optimization leading to optimality. The optimal initial forcing can thus be found by $\mathbf{u}_0^* = \mathbf{C}_N^{-1}\,\mathbf{y}_{N,0}^*$, and therefore $\mathbf{x}^*(0) = \mathbf{B}\,\mathbf{u}_0^* = \mathbf{B}\,\mathbf{C}_N^{-1}\,\mathbf{y}_{N,0}^*$. As for G, the optimal $H_{\max} = \max_t H(t)$ occurs at $t = t^*$. The optimal initial input vector $\mathbf{u}_0^*$ can be found from the SVD of

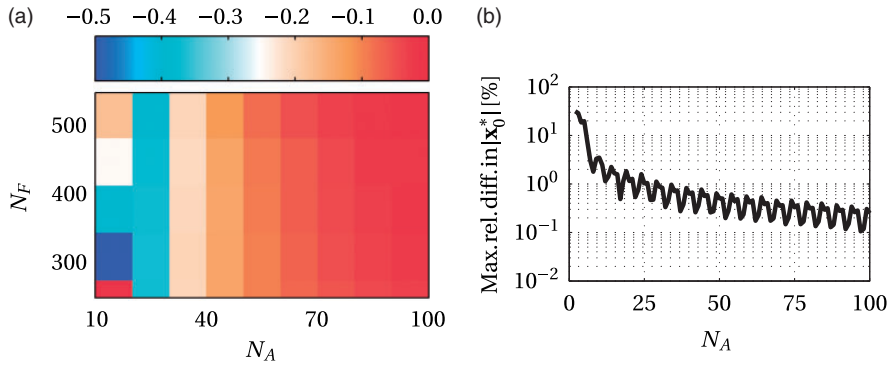

Figure 6. (a) Relative difference of $H_{\max}$ (%) as a function of the number of basis functions N_A (and thus N_F). The reference value of $H_{\max} \approx 1.6$ is taken at the finest resolution $N_A = 100$ (corresponding to $N_F = 550$). (b) Maximum of the relative difference (%) between $|\mathbf{x}_0^*|$ with N_A and $N_A - 1$ as a function of N_A. Configuration: $\kappa_0 = 0$, $K = 7.3 \times 10^{-4}$, default parameter values.

$\mathbf{C}\exp(\mathbf{A}t^*)\mathbf{B}\mathbf{C}_N^{-1}$, where $\mathbf{u}_0^*$ corresponds to the first right-singular vector pre-multiplied by $\mathbf{C}_N^{-1}$.

In analogy to the definition of G in equation (33), H in equation (38) also describes an optimization problem of *normalized* output energy for autonomous systems. However, the important advantage of H over G lies in the fact that it can be effectively used to compute the optimal *relative* amplification of energy $\mathcal{G}$ using SVD even if the output energy E defines a semi-norm. The procedure to find $\mathcal{G}_{\max}$ via optimization of H is explained in the following.

The definition of $\mathbf{B}$ as detailed above equation (38) allows to control the impact of the states of different subsystems onto the initial condition $\mathbf{x}(0) = \mathbf{B}\mathbf{u}_0$. This is done by varying the magnitude of the diagonal submatrices in $\mathbf{B}$ that relate to each subsystem. We thereby implicitly weight the contribution of each subsystem onto the initial levels of output and kernel energy, E_0 and $E_0^\dagger$, respectively (see equation (34)). For the example of the thermoacoustic model with the two subsystems acoustics/flow and flame as defined in The generic thermoacoustic model section, the definition of

$$\mathbf{B} = \begin{bmatrix} k_1\mathbf{I} & \mathbf{0} \\ \mathbf{0} & k_2\mathbf{I} \end{bmatrix}$$

will lead to zero initial kernel energy $E_0^\dagger = 0$ for $k_1 = 1$ and $k_2 = 0$, and to zero initial output energy $E_0 = 0$ for $k_1 = 0$ and $k_2 = 1$. According to equation (35), the latter two limiting cases correspond to an initial ratio of kernel to output energy $\kappa_0 = 0$ and $\kappa_0 = \infty$, respectively. In the special case of $k_1 = k_2 = 1$, H is equivalent to G, and applying SVD to equation (38) yields the OIC $\mathbf{x}^*(0) = \mathbf{u}_0^*$, as well as the corresponding optimal initial ratio of kernel to output energy κ_0^* for which the normalized output energy is maximized.

In summary, variation of $\mathbf{B}$ amounts to optimizing for the maximum amplification of output energy as a function of the constrained kernel space. It is thus possible to compute $H_{\max}$ and the optimal evolution of output energy $E^*(t)$ over the entire range of κ_0. From there, it is straightforward to compute the corresponding maximum *relative* amplification of output energy $\mathcal{G}_{\max} = E^*(t = t^*)/E_0$. Although this approach requires multiple optimization runs, it is easy to implement and for low-order models represents a computationally inexpensive alternative to variational methods.

Analysis of non-normal transient growth around a stable fix point

This section analyzes the non-normal transient growth observed in the thermoacoustic model introduced in The low-order thermoacoustic model section. Since the output energy defines a semi-norm, we investigate the influence on transient growth of those initial states that are not contained in the output energy, and how the optimal normalized energy amplification $H_{\max}$ and the optimal mode shapes evolve in time (see Dynamics of non-normal transient growth section). The influence of different model parameters on transient growth is addressed in the Parameters influencing transient growth section. By default and unless otherwise mentioned, the strength of the fluctuating heat source K is set to approximately 99 % of the critical value K_{crit} at the linear stability bound.

Before proceeding, it is necessary to ensure that the results presented in the following are independent of the resolution of the numerical schemes used. In Figure 6(a), we investigate the value of $H_{\max}$ obtained when varying the number of basis functions N_A used in the model of the acoustics/flow subsystem. Since N_F used in the model of the flame subsystem is linked to N_A by a condition ensuring numerical stability, $N_F \propto (N_A, \mathrm{Sr}, \Delta_\beta, M_u)$, variation of N_A accordingly changes N_F. The color shading indicates the difference in $H_{\max}$ relative to the finest resolution in the in the top right

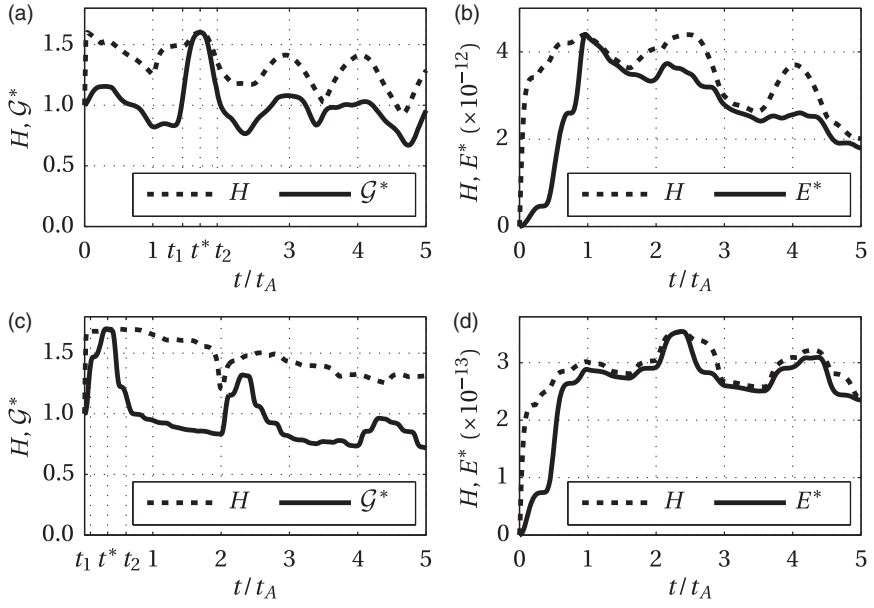

Figure 7. Left column: Time traces of the maximum normalized output energy H defined in equation (4) (- - -) and optimal relative energy amplification $\mathcal{G}^*$ defined in equation (4) (—) in the limiting case of $\kappa_0 = 0$ (i.e. no kernel energy at $t = 0$). Right column: Same as left column, but for $\kappa_0 = \infty$. In this case, $E_0 = 0$ and we plot the optimal amplification of output energy E^* (—). Damping is given by the default (top row) and the minimum parameter values (bottom row) shown in Table 1. Configuration: $K = 7.3 \times 10^{-4}$ and $K = 1.8 \times 10^{-4}$ for default and low damping values, respectively, otherwise default parameter values.

corner of the plot. It is visible that $H_{\max} \approx 1.6$ changes by less than 0.1% for $N_A > 50$.

The maximum of the relative difference between $|\mathbf{x}_0^*|$ with N_A and $N_A - 1$ basis functions is shown in Figure 6(b) as a function of increasing N_A. For $N_A > 30$, the coarse-grained slope of this error measure is below 1%. To ensure independence from the numerical resolution, all following results are produced with $N_A = 70$ unless otherwise mentioned. Under default parameter values, this corresponds to $N_F = 414$.

The dynamics of non-normal transient growth

The effect of kernel energy. Since the output energy E of the discrete model $(\mathbf{A}^{(T)}, \mathbf{C}^{(T)})$ of $\mathcal{S}^{(T)}$ defines a seminorm, the initial ratio of kernel to output energy κ_0 should be taken into account as an additional optimization parameter to find the optimal relative amplification of output energy $\mathcal{G}_{\max} = E_{\max}/E_0$ (see also the discussion in the Optimization of output energy using SVD section).

The first limiting case is that of $\kappa_0 = 0$, where the initial condition does not contain fluctuations in the heat source subsystem $\mathcal{S}^{(F)}$. The corresponding time traces of the maximum normalized energy amplification H (defined in equation (38)) and optimal relative energy amplification $\mathcal{G}^*$ (defined in equation (31)) are plotted in Figure 7(a) and (c) for default and minimum values of damping, respectively. For default damping values, $H_{\max} \approx 1.6$ is reached at $t^* = 1.69$ acoustic time scales. For low damping, $H_{\max} \approx 1.7$ occurs very quickly at $t^* = 0.34$ acoustic time scales.

The other limiting case is obtained for $\kappa_0 = \infty$, where the initial output energy $E_0 = 0$ and thus $\mathcal{G}_{\max} = \infty$. In this case, the optimal initial condition $\mathbf{x}_0^{*(T)}$ contains non-zero entries only in $\mathbf{x}_0^{(F)}$, which subsequently affect the acoustic field (and thus the output energy E) for $t > 0$. This corresponds to an initial condition where the heat source is perturbed in a quiescent acoustic environment (for example, by oscillating the flame holder without this action generating noise). The time traces of the maximum normalized output energy H and the optimal output energy E^* corresponding to this limiting case are plotted in Figure 7(b) and (d) for default and minimum values of damping, respectively. It can be seen that $E_0 = 0$ increases up to $E_{\max} = H_{\max}$ at optimality for $t = t^*$.

In practice, it is not possible to generate initial conditions that are exclusively affecting only one of the subsystems. It is therefore interesting to investigate how the initial ratio of kernel to output energy κ_0 affects the maximum levels of non-normal transient growth. Using the optimization procedure laid out in the Optimization of output energy using SVD section, we compute the maximum relative and normalized amplification of output energy $\mathcal{G}_{\max}$ and $H_{\max}$, respectively, over a range of κ_0. As κ_0 is reduced, the initial level of output energy E_0 increases. This decreases the available amount of kernel energy that could potentially be converted to output energy through the

coupling between both subsystems. One might therefore expect that the maximum relative energy amplification $\mathcal{G}_{\max}$ increases monotonically with κ_0, as shown by Foures et al.[34] for a model of a viscous turbulent flow. For the present model describing $\mathcal{S}^{(T)}$, however, $\mathcal{G}_{\max}$ is not a monotone function of κ_0. As can be seen from Figure 8, $\mathcal{G}_{\max} \approx H_{\max} \approx 1.6$ for $0 \leq \kappa_0 < 10^3$. For $\kappa_0 > 10^3$, $H_{\max}$ tends to infinity, whereas $\mathcal{G}_{\max}$ decreases to values slightly above unity, before finally tending to the anticipated maximum of infinity for $\kappa_0 > 10^{10}$.

Although the initial output energy E_0 indeed decreases for increasing κ_0, the effect of $\mathcal{S}^{(F)}$ onto $\mathcal{S}^{(A)}$ is not sufficiently strong so as to convert large parts of the kernel energy to output energy. This is due to the Rayleigh source term given in the first row of equation (30b), which dictates that the conversion from kernel to output energy can only take place if the acoustic field is receptive to fluctuations in heat release rate. Otherwise, the interaction of both subsystems does not modify or even decreases E, and kernel energy is not converted to output energy. This effect is fundamentally different from flow systems, where the entire kernel energy eventually transfers to output energy.[34]

The behavior of $\mathcal{G}_{\max}$ with respect to κ_0 indicates that the OICs with non-zero initial output energy E_0 are dominated by non-zero values in the state vector $\mathbf{x}_0^{(A)}$ of the acoustics subsystem $\mathcal{S}^{(A)}$. Since the Rayleigh term inhibits conservative transfer of kernel to output energy, initial perturbations in the heat source subsystem $\mathcal{S}^{(F)}$ are not very effective at maximizing the acoustic energy. As mentioned above, for all practical setups, the initial output energy $E_0 > 0$, and thus $\kappa_0 \ll \infty$. In addition, $\mathcal{G}_{\max} \approx H_{\max} \approx 1.6$ is unaffected by the magnitude of the initial kernel energy over a wide range of κ_0. This translates to small perturbations in the heat source subsystem $\mathcal{S}^{(F)}$ not causing a significant change in the dynamics of non-normal transient growth of $\mathcal{S}^{(T)}$. We therefore focus further analysis onto the limiting case of $\kappa_0 = 0$ (i.e. the initial condition does not contain any fluctuations in the heat source subsystem $\mathcal{S}^{(F)}$). This also facilitates interpretation of results, as the relative equals the normalized amplification of output energy, $\mathcal{G}(t) = H(t) = G(t)$.

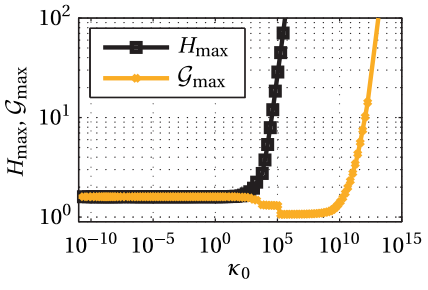

Figure 8. Maximum normalized and relative amplification of output energy, $H_{\max}$ and $\mathcal{G}_{\max}$, respectively, as a function of the initial ratio of kernel to output energy κ_0. For $\kappa_0 < 10^3$, $\mathcal{G}_{\max} \approx H_{\max} \approx 1.6$. For $\kappa_0 > 10^3$, $H_{\max}$ tends to infinity, whereas $\mathcal{G}_{\max}$ decreases and only tends to infinity for $\kappa_0 > 10^{10}$. Configuration: $K = 7.3 \times 10^{-4}$, default parameter values.

The process of non-normal transient growth. The evolution of the acoustic states $x_A = [v(\xi), p(\xi)]^T$ and the flame states $x_F = v_F(t-\tau)$ during the occurrence of non-normal transient growth is visualized in Figure 9 for the default and low damping values specified in Table 1. Four snapshots in time are depicted, each corresponding to the optimal evolution of relative amplification of output energy $\mathcal{G}^*$ shown in the left column of Figure 7: the OIC at $t=0$, the phase of dominant transient growth at $t=t_1$, optimality at $t = t^*$, and the phase of decay following $H_{\max}$ at $t = t_2$.

The OIC at $t=0$ is not instructive as such, but it sets the stage for the phase of growth leading to the optimal energy amplification. This process is analyzed in the following in the context of the flux and source terms driving the temporal evolution of output energy. Since $M=0.05$ is very small, we neglect the corresponding flux and source terms in equation (30). With this simplification, and as discussed in The output of the low-order thermoacoustic model section, transient growth can be explained by two driving source terms, the Rayleigh source term resulting from the interaction of the acoustic field with the heat source, and the inherent source term resulting from the assumption of a flame at rest. In order to lead to an increase in output energy, driving needs to overcome the strictly dissipative damping term.

For low damping values, the optimal energy amplification $H_{\max}$ occurs at $t^* = 0.34$ acoustic time scales. By this time, the fluctuations in velocity at the flame base have not yet been advected to the tip of the flame, where the dominant flame response in $\dot{q}$ is generated. For reference, the shape of the IR function of the premixed wedge flame discussed in The flame subsystem section is overlaid onto the lagged values of velocity fluctuations at the flame base $v_F(t-\tau)$ in the right column of Figure 9. Non-zero $v_F(t-\tau)$ (indicated by the yellow lines) does not encounter the region of strong flame response in any of the snapshots. Thus no significant fluctuations in heat release rate $\dot{q}$ are generated (see also the convolution equation (17) governing the output of the flame subsystem), and the Rayleigh source term is negligible. On the other hand, the inherent source term is positive if $v(\xi_F)$ and $p(\xi_F)$ are of opposite sign. This is the case during the driving phase at $t = t_1$. At optimality, $\mathrm{d}E/\mathrm{d}t = 0$, and the net source terms are zero. During the phase of

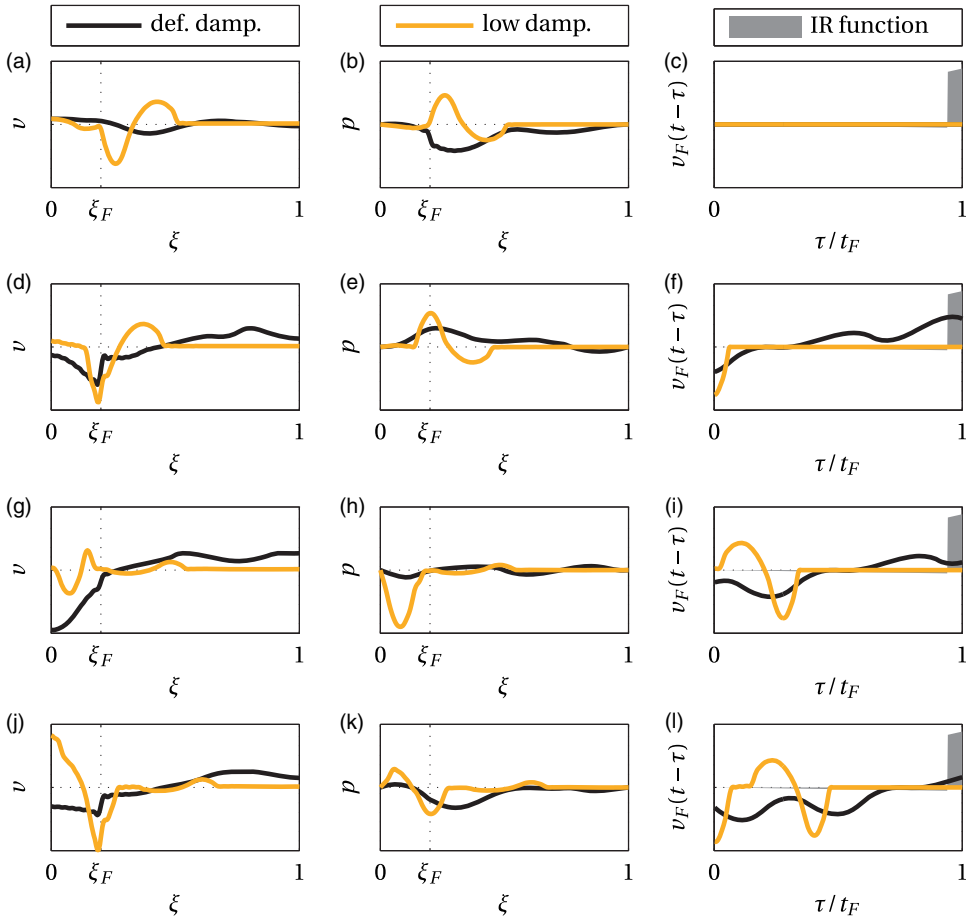

Figure 9. Profiles of $v(\xi)$, $p(\xi)$ and $v_F(t-\tau)$ (left, center and right columns, respectively) during non-normal transient growth for default (—) and low damping (—): (a) The OIC at $t=0$, (b) the phase of dominant transient growth at $t=t_1$, (c) optimality at $t=t^*$, and (d) the phase of decay at $t=t_2$ (all snapshots are indicated in Figure 7). The IR function is overlaid in the right column. Configuration: $\kappa_0=0$, $K=7.3\times10^{-4}$ and $K=1.8\times10^{-4}$ for default and low damping, respectively, otherwise default parameter values.

decay at $t=t_2$, $v(\xi_F)$ and $p(\xi_F)$ are of same sign and thus the output energy E decreases more strongly than solely by the action of dissipative damping.

For default damping values, the optimal energy amplification $H_{\max}$ occurs at $t^*=1.69$ acoustic time scales. In contrast to the case with low damping, the phase of dominant transient growth is due to both source terms driving the output energy in parallel, as can be seen from the black lines in the second row of Figure 9. At $t=t_1$, $v(\xi_F)$ and $p(\xi_F)$ are of opposite sign. Also, dominant non-zero values of the lagged acoustic velocity at the flame base $v_F(t-\tau)$ meets the dominant zone of the IR function, thus generating significant $\dot{q}$, that in turn is of the same sign as $p(\xi_F)$. The Rayleigh source term is hence positive. At optimality, the net source terms are zero as before. During the phase of decay at $t=t_2$, $v(\xi_F)$ and $p(\xi_F)$ are of the same sign, whereas $\dot{q}$ and $p(\xi_F)$ are of opposite sign. In addition to damping mechanisms, both source terms thus contribute to decay in output energy.

In summary, the OIC is such that the source terms driving the output energy are maximized during a short period of time. We can distinguish two scenarios of *optimal* non-normal transient growth, which are discussed in the following.

If optimality is reached at time scales much shorter than the characteristic time scales of the flame subsystem, that is, at an acoustic time scale, non-normal transient growth is due to the inherent modeling assumption of a flame at rest. In the present low-order model, this scenario is observed for low damping values. As mentioned in the discussion following the second example in The output defines the perspective section, the inherent scenario of non-normal transient growth is physical as such. However, the modeling assumption of a flame at rest, strictly speaking, is not physical.

If optimality is reached at time scales of the order of or larger than the characteristic time scales of the flame subsystem, optimal non-normal transient growth is due

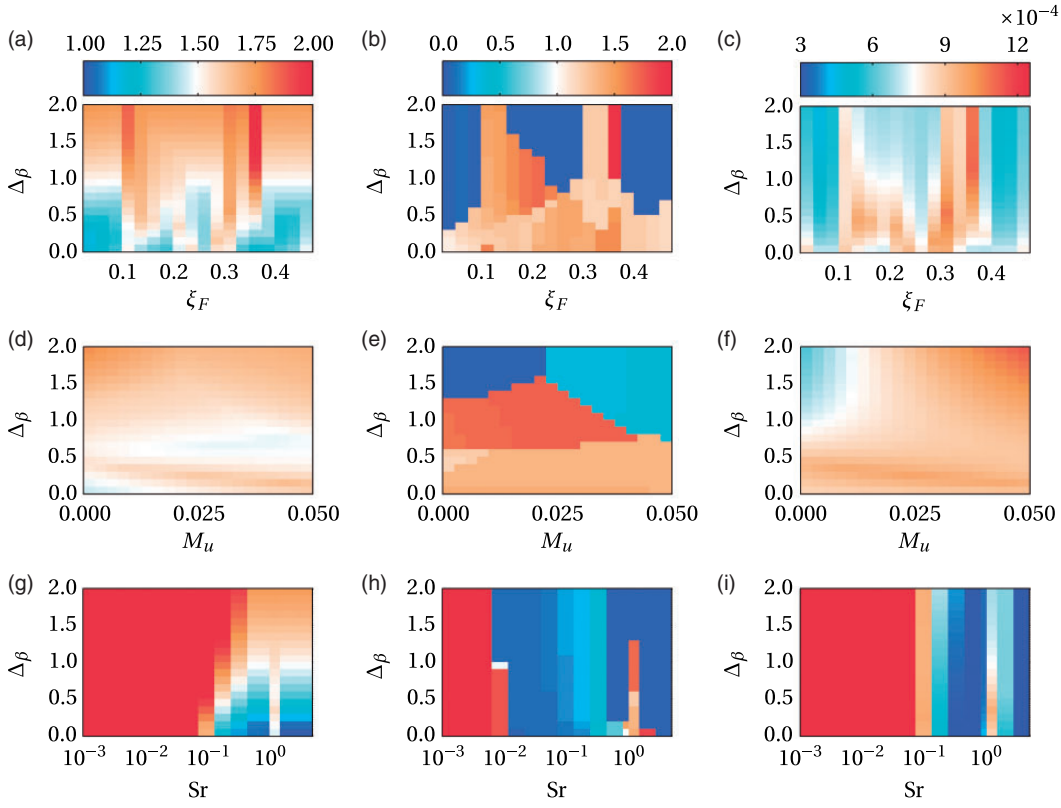

Figure 10. The optimal energy amplification H_{max} (first column), the time at optimality t^* (second column), and K_{crit} (third column) of the autonomous thermoacoustic model (**A**,**C**) in different 2-parameter spaces with $\kappa_0 = 0$, $K \approx 0.99\,K_{crit}$, and otherwise default parameter values: (a) to (c) Δ_β vs. ξ_F, (d) to (f) Δ_β vs. M_u, (g) to (i) Δ_β vs. Sr.

to the interaction of the heat source with the acoustic field. This second scenario represents a physical event of non-normal transient growth in thermoacoustic systems. It is observed in the present low-order model for default damping conditions.

Despite the physical nature of the second scenario of non-normal transient growth, transient growth originating from the temperature gradient as in the first scenario is also present. As shown in Figure 7(a), transient growth can already occur for very small times (i.e. $H > 1$ for $t > 0^+$). This indicates that both scenarios of non-normal transient growth occur in parallel. For this configuration, however, the largest (i.e. optimal) transient growth is due to the physical coupling of the heat source with the acoustic field.

Parameters influencing transient growth

In the following, we analyze the influence of several parameters of the thermoacoustic model on non-normal transient growth: the position of the flame, the temperature jump, mean flow, and the ratio of time scales between the two subsystems (respectively given by the model parameters ξ_F, Δ_β, M_u and Sr). The effect of the other model parameters is omitted in the present work for brevity of presentation. A detailed treatment can be found in Blumenthal.[41]

The optimal normalized energy amplification H_{max} and the time at optimality t^* are displayed in a two-parameter space in the first two columns of Figure 10. To ease comparison, the first parameter is always given by the temperature incremental factor Δ_β. In parallel, we plot the corresponding linear stability maps in the third column of Figure 10. The latter are determined by finding the critical strength of the heat source $K = K_{crit}$ at which the system is marginally stable. Regions of increased values of K_{crit} thus indicate more stable system configurations. Marginal stability is reached when the largest growth rate of the eigenvalues of the discrete state matrix **A** approaches zero. In this manner, it is possible to verify the above statement on whether the maximum levels of non-normal transient growth are related to the critical strength of the flame K_{crit} at the linear stability bound (see the discussion in the end of The output of the low-order thermoacoustic model section).

The effect of a temperature jump on H_{max} and especially on t^* is strong, which is in agreement with the studies of Zhao et al.[57,58] In general, low and intermediate values of Δ_β favor the physical second scenario of

transient growth via the Rayleigh term. For high Δ_β, transient growth more likely occurs through the inherent first scenario, as the source term resulting from the gradient in temperature at ξ_F is increased. However, the temperature jump does not alter the order of magnitude of maximum non-normal transient growth.

Regarding the flame position ξ_F, the optimal energy growth $H_{\max}$ is more pronounced in the surroundings of $\xi_F \approx 0.1$ and $\xi_F \approx 0.35$. In these regions, t^* is also large, indicative of the physical second scenario of transient growth via the Rayleigh term. By inspection of the linear stability map shown in Figure 10(c), it is noticeable that regions of large $H_{\max}$ align well with regions of enhanced linear stability, where K_{crit} is large. This also hints at the second scenario, because enhanced linear stability goes in hand with the system being able to bear a stronger fluctuating heat source before becoming linearly unstable, and thus a stronger Rayleigh term. The results for $\xi_F > 0.5$ (i.e. in the downstream part of the duct) are not shown because they do not provide any further insights.

The effect of mean flow on $H_{\max}$ and on t^* is barely noticeable in the range of upstream Mach numbers considered. The simplifying assumption of neglecting the flux and source terms that depend on M_u, and thus to explain non-normal transient growth with only two dominant source terms, is therefore valid.

However, the Strouhal number Sr, that is the ratio of time scales between the subsystems flame and acoustics/flow plays a crucial role for non-normal transient growth (see Figure 10(g) to (i)). In general, $H_{\max}$ decreases with Sr. For large Strouhal numbers (except for $\text{Sr} = 1$), which are those encountered in many thermoacoustic systems, $H_{\max}$ and t^* are small. This behavior is indicative of the inherent first scenario of transient growth, where the interaction of the heat source and the acoustic field is negligible. On the other hand, transient growth through the physical second scenario via the Rayleigh term is extremely pronounced for very low Strouhal numbers. For example, at $\text{Sr} = 10^{-3}$, $H_{\max} \approx 20$, which exceeds the maximum color shading by an order of magnitude. Optimality is reached at the order of two acoustic time scales.

As observed for ξ_F, ranges of Sr with the physical second scenario of transient growth align well with regions of enhanced linear stability (see Figure 10(i)). Since the system can bear a stronger heat source before becoming linearly unstable, the Rayleigh term leading to non-normal transient growth is also stronger. This is the case for small characteristic time scales of the flame subsystem (i.e. small Sr), which tend to stabilize the thermoacoustic system. Conversely, heat sources with large characteristic time scales tend to be detrimental for the stability of the thermoacoustic system. It is well known from control theory that systems with large delays are more difficult to control,[42] because a change in the delayed part of the system shows its effect only after some time lag. By the time the effect of a slow heat source is thus noticeable in a thermoacoustic configuration, damping mechanisms have already significantly diminished the amplitude levels of the acoustic field.

In summary, optimal non-normal transient growth thus results from a maximization of the source and flux terms associated with the definition of the thermoacoustic model. This observation was anticipated by analytical arguments in The output of the low-order thermoacoustic model section. For the present model, the transient maximization of source terms either leads to the advent of inherent transient growth (due to the modeling assumption of a flame at rest), or to the advent of physical transient growth with a transiently maximized Rayleigh term. Thermoacoustic configurations that can bear a stronger heat source (i.e. more stable configurations) can thus exhibit larger levels of non-normal transient growth. This is especially well visible in the present model for certain values of the position of the heat source ξ_F, and for extremely low values of Strouhal number Sr.

Synopsis

The present work formulates a model of a thermoacoustic system as a generic multi-physics system consisting of two subsystems in feedback (acoustics/flow and flame). The different subsystems are described by analytical and semi-analytical models for the subsystems acoustics/flow (the linearized Euler equations) and flame (the G-equation framework). The analysis of the thermoacoustic model involves the study of output energy and the dynamics of physical non-normal transient growth around a stable fix point.

The novelty of the present work consists in a rigorous systems-based approach towards the study of non-normal transient growth in thermoacoustics. The theoretical framework presented above allows for energy metrics that can describe semi-norms, while still resorting to the simple and computationally inexpensive optimization routine of singular value decomposition. This provides for great flexibility in investigating any kind of energy norm. In addition, the low-order thermoacoustic model includes a mean temperature jump, a trivial, but non-zero mean flow, and a heat source with time-distributed response characteristics, of which the time lags need not be small with respect to the acoustic time scales.

The systemic approach is also applied to the question of energy norm in thermoacoustics. We argue that the definition of energy norm is to a considerable extent a matter of choice, but one that is critically tied to the dynamics described by the system model. The energy

metric merely prescribes the perspective from which non-normal transient growth needs to be interpreted. To this regard, the energy metric is a crucial factor for investigating non-normal transient growth. However, it does not alter the degree of non-normality as such.

For the investigated thermoacoustic model, we choose to use the acoustic energy as energy measure. The latter describes a semi-norm, because it only includes contributions from the acoustic field, but not from the flame. Optimizing for optimal non-normal transient growth therefore opens the need to investigate the effect of how initial perturbations in the flame affect the evolution of acoustic energy. It is shown that the initial perturbations in the flame are not dominantly influential for transient growth, but that optimal non-normal transient growth is mostly due to non-zero initial perturbations in the acoustic field (unless all initial perturbations are contained in the flame). This marks a strong difference to hydrodynamic systems, where initial perturbations that are not contained in the energy metric affect the evolution of energy in a conservative manner.

Non-normal transient growth is further shown to result from a transient maximization of the source and flux terms associated with the definition of the autonomous model (i.e. the dynamics together with the definition of output). For the employed model of a flame enclosed in a duct, we identify two scenarios of non-normal transient growth, of which one is inherent to the modeling assumption of a flame at rest, and the other is related to a transient maximization of the classical Rayleigh term. Non-normal transient growth is thus more pronounced in configurations that can bear a stronger fluctuating heat source, because this increases the magnitude of the Rayleigh term. It is shown that the characteristic time scale of the flame subsystem is a crucial parameter for the magnitude of non-normal transient growth, because it influences the linear stability characteristics of a thermoacoustic system in a dominant manner. Heat sources with fast response times are prone to larger levels of non-normal transient growth, whereas non-normal transient growth is marginal for slow-reacting heat sources.

In future studies, it will be interesting to investigate the effect of non-normality onto other thermoacoustic setups. Owing to the generic systems approach laid out in the present study, it is straightforward to redo the present analysis for different and perhaps more sophisticated models of existing subsystems, and/or by including other subsystems.

Acknowledgements

We thank the reviewers of this paper for the fruitful discussions throughout the reviewing process, which have significantly contributed to increasing the quality of results and presentation.

Declaration of conflicting interests

The author(s) declared no potential conflicts of interest with respect to the research, authorship, and/or publication of this article.

Funding

The author(s) disclosed receipt of the following financial support for the research, authorship, and/or publication of this article: Financial support was provided by the Technische Universität München – Institute for Advanced Study, funded by the German Excellence Initiative. The authors also gratefully acknowledge the financial support by the German Research Foundation DFG, project PO 710/12-1.

References

1. Schmid PJ and Henningson DS. *Stability and transition in shear flows*. New York, NY, USA: Springer Verlag, 2001.
2. Chagelishvili G, Chanishvili R and Lominadze D. Physics of the amplification of vortex disturbances in shear flows. *JETP Lett* 1996; 63: 543–549.
3. Farrell BF and Ioannou PJ. Generalized stability theory. Part I: Autonomous operators. *J Atmos Sci* 1996; 53: 2025–2040.
4. Farrell BF and Ioannou PJ. Generalized stability theory. Part II: Nonautonomous operators. *J Atmos Sci* 1996; 53: 2041–2053.
5. Reddy SC, Schmid PJ and Henningson DS. Pseudospectra of the Orr-Sommerfeld operator. *SIAM J Appl Math* 1993; 53: 15–47.
6. Schmid PJ. Nonmodal stability theory. *Ann Rev Fluid Mech* 2007; 39: 129–162.
7. Trefethen LN, Trefethen AE, Reddy SC, et al. Hydrodynamic stability without eigenvalues. *Science* 1993; 261: 578–584.
8. Balasubramanian K and Sujith RI. Non-normality and nonlinearity in combustion acoustic interaction in diffusion flames. *J Fluid Mech* 2008; 594: 29–57.
9. Balasubramanian K and Sujith RI. Non-normality and nonlinearity in combustionacoustic interaction in diffusion flames CORRIGENDUM. *J Fluid Mech* 2013; 733: 680–680.
10. Balasubramanian K and Sujith RI. Thermoacoustic instability in a Rijke tube: non-normality and nonlinearity. *Phys Fluid* 2008; 20: 044103.
11. Kedia KS, Nagaraja SB and Sujith RI. Impact of linear coupling on thermoacoustic instabilities. *Combust Sci Technol* 2008; 180: 1588–1612.
12. Nagaraja S, Kedia K and Sujith RI. Characterizing energy growth during combustion instabilities: singular values or eigenvalues? *Proc Combust Inst* 2009; 32: 2933–2940.
13. Subramanian P and Sujith RI. Non-normality and internal flame dynamics in premixed flame-acoustic interaction. *J Fluid Mech* 2011; 679: 315–342.
14. Mangesius H and Polifke W. A discrete-time, state-space approach for modelling non-normal effects in thermoacoustic systems. *Int J Spray Combust Dynam* 2011; 3: 331–350.

15. Juniper MP. Triggering in the horizontal Rijke tube: non-normality, transient growth and bypass transition. *J Fluid Mech* 2011; 667: 272–308.
16. Juniper MP. Triggering in thermoacoustics. *Int J Spray Combust Dynam* 2012; 4: 217–238.
17. Wieczorek K, Sensiau C, Polifke W, et al. Assessing non-normal effects in thermoacoustic systems with mean flow. *Phys Fluid* 2011; 23: 107103.
18. Magri L, Balasubramanian K, Sujith RI, et al. Non-normality in combustion-acoustic interaction in diffusion flames: a critical revision. *J Fluid Mech* 2013; 733: 681–683.
19. Juniper MP. Transient growth and triggering in the horizontal Rijke tube. *Int J Spray Combust Dynam* 2011; 3: 209–224.
20. Gebhardt T and Grossmann S. Chaos transition despite linear stability. *Phys Rev E* 1994; 50: 3705–3711.
21. Grossmann S. The onset of shear flow turbulence. *Rev Modern Phys* 2000; 72: 603–618.
22. George KJ and Sujith R. On Chu's disturbance energy. *J Sound Vibrat* 2011; 330: 5280–5291.
23. George KJ and Sujith RI. Disturbance energy norms: a critical analysis. *J Sound Vibrat* 2012; 331: 1552–1566.
24. Culick FEC. A note on ordering perturbations and the insignificance of linear coupling in combustion instabilities. *Combust Sci Technol* 1997; 126: 359–377.
25. Durox D, Schuller T, Noiray N, et al. Rayleigh criterion and acoustic energy balance in unconfined self-sustained oscillating flames. *Combust Flame* 2009; 156: 106–119.
26. Giauque A, Nicoud F and Brear M. Numerical assessment of stability criteria from disturbance energies in gaseous combustion. In: *13th AIAA/CEAS aeroacoustics conference*, Rome, Italy, 21–23 May, 2007.
27. Testud P, Aurégan Y, Moussou P, et al. The whistling potentiality of an orifice in a confined flow using an energetic criterion. *J Sound Vibrat* 2009; 325: 769–780.
28. Aurégan Y and Starobinski R. Determination of acoustical energy dissipation/production potentiality from the acoustical transfer functions of a multiport. *Acta Acustica Unite Acustica* 1999; 85: 788–792.
29. Polifke W. Thermo-acoustic instability potentiality of a premix burner. In: *European combustion meeting*, July 2011. Cardiff, UK: British Section of the Combustion Institute.
30. Giauque A, Poinsot T, Brear M, et al. Budget of disturbance energy in gaseous reacting flows. In: *Proceedings of the summer program 2006*, Center for Turbulence Research, pp. 285–297.
31. Chu BT. On the energy transfer to small disturbances in fluid flow (Part I). *Acta Mech* 1965; 1: 215–234.
32. Blumenthal RS, Subramanian P, Sujith RI, et al. Novel perspectives on the dynamics of premixed flames. *Combust Flame* 2013; 160: 1215–1224.
33. Cantrell RH and Hart RW. Interaction between sound and flow in acoustic cavities: mass, momentum, and energy considerations. *J Acoust Soc Am* 1964; 36: 697.
34. Foures DPG, Caulfield CP and Schmid PJ. Variational framework for flow optimization using seminorm constraints. *Phys Rev E* 2012; 86: 026306.
35. Magri L. *Adjoint methods in thermo-acoustic and combustion instability*. PhD Thesis, Cambridge University, 2015.
36. Jiménez J. *Localized amplification of energy in turbulent channels*. Center for Turbulence Research, Annual Research Briefs, 2009.
37. Mariappan S and Sujith RI. Thermoacoustic instability in a solid rocket motor: non-normality and nonlinear instabilities. *J Fluid Mech* 2010; 653: 1–33.
38. Myers MK. Transport of energy by disturbances in arbitrary steady flows. *J Fluid Mech* 1991; 226: 383–400.
39. Poinsot T and Veynante D. *Theoretical and numerical combustion*, 2nd ed. Philadelphia, PA: R T Edwards Inc, 2005.
40. Rienstra SW and Hirschberg A. *An introduction to acoustics*. Einhoven University of Technology, 2014.
41. Blumenthal RS. *A systems view on non-normal transient growth in thermoacoustics*. PhD Thesis, Eindhoven, The Netherlands: TU München, 2015.
42. Tangirala AK. *Principles of system identification: theory and practice*. Boca Raton, FL: Taylor & Francis, 2014.
43. Boyer L and Quinard J. On the dynamics of anchored flames. *Combustion and Flame* 1990; 82: 51–65.
44. Fleifil M, Annaswamy AM, Ghoneim ZA, et al. Response of a laminar premixed flame to flow oscillations: a kinematic model and thermoacoustic instability results. *Combust Flame* 1996; 106: 487–510.
45. Schuller T, Durox D and Candel S. A unified model for the prediction of laminar flame transfer functions: comparisons between conical and V-flame dynamics. *Combust Flame* 2003; 134: 21–34.
46. Ducruix S, Durox D and Candel S. Theoretical and experimental determinations of the flame transfer function of a laminar premixed flame. *Symposium (International) on Combust* 2000; 28: 765–773.
47. Kashinath K, Waugh IC and Juniper MP. Nonlinear self-excited thermoacoustic oscillations of a ducted premixed flame: bifurcations and routes to chaos. *J Fluid Mech* 2014; 761: 399–430.
48. Polifke W. System identification for aero- and thermo-acoustic applications. In: Schram C (ed.) *Advances in aero-acoustics and thermo-acoustics*. Rhode-St-Genèse, BE: Von Karman Institute, 2011, pp.1–46.
49. Subramanian P, Blumenthal RS, Polifke W, et al. Distributed time lag response functions for the modelling of combustion dynamics. *Combust Theory Model* 2015; 19: 223–237.
50. Schmid M, Blumenthal RS, Schulze M, et al. Quantitative stability analysis using real frequency response data. *J Eng Gas Turbine Power* 2013; 135: 121601.
51. Selimefendigil F, Sujith RI and Polifke W. Identification of heat transfer dynamics for non-modal analysis of thermoacoustic stability. *Applied Mathematics and Computation* 2011; 217: 5134–5150.
52. Kashinath K. *Nonlinear thermoacoustic oscillations of a ducted laminar premixed flame*. PhD Thesis, University of Cambridge, 2013.
53. Nicoud F and Wieczorek K. About the zero Mach number assumption in the calculation of thermoacoustic instabilities. *Int J Spray Combust Dynam* 2008; 1: 67–111.
54. Bauerheim M, Nicoud F and Poinsot T. Theoretical analysis of the mass balance equation through a flame at zero and non-zero Mach numbers. *Combustion and Flame* 2015; 162: 60–67.

55. Strobio Chen L, Bomberg S and Polifke W. Propagation and generation of acoustic and entropy waves across a moving flame front. *Combust Flame* 2016; 166: 170–180.
56. Kim J and Bewley TR. A linear systems approach to flow control. *Ann Rev Fluid Mech* 2007; 39: 383–417.
57. Zhao D. Transient growth of flow disturbances in triggering a Rijke tube combustion instability. *Combust Flame* 2012; 159: 2126–2137.
58. Li X and Zhao D. Mean temperature effect on a thermoacoustic system stability and non-normality. *Low Frequency Noise, Vibrat Active Control* 2015; 34: 185–200.
59. Culick FEC. *Unsteady motions in combustion chambers for propulsion systems*. Number AC/323(AVT-039)TP/103 in RTO AGARDograph, 2006.
60. Culick FEC. Spatial averaging combined with a perturbation/iteration procedure. *Int J Spray Combust Dynam* 2012; 4: 185–216.
61. Matveev KI and Culick FEC. A model for combustion instability invovling vortex shedding. *Combust Sci Technol* 2003; 175: 1059–1083.
62. Kashinath K, Hemchandra S and Juniper MP. Nonlinear phenomena in thermoacoustic systems with premixed flames. *J Eng Gas Turbine Power* 2013; 135: 061502.
63. Mariappan S and Sujith RI. Modelling nonlinear thermoacoustic instability in an electrically heated rijke tube. *J Fluid Mech* 2011; 680: 511–533.

Appendix

Notation

$\mathcal{A}$, **A**	continuous system operator and discrete system matrix
$\mathcal{B}$, **B**	continuous input operator and discrete input matrix
$\mathcal{C}$, **C**	continuous output operator and discrete output matrix
D	1-D spatial profile of heat addition (1/m)
$\mathcal{E}$, E	continuous output energy and discrete output energy
F	flux term
G	maximum normalized output energy of an autonomous model (–)
$\mathcal{G}$	relative amplification of output energy (–)
H	impulse response function
H	maximum normalized output energy of a forced system (–)
K	kernel space weighting factor
K	non-dimensional strength of heat source (–)
K_0	control parameter scaling the strength of heat source given by K (–)
L	length (m)
N	normal vector
N	number of states
M	number of inputs; Mach number (–)
P	pressure (N/m^2)
P	number of outputs
R_F	flame radius (m)
$\dot{q}$	heat release rate (W)
s, S	specific and integral source term
Sr	Strouhal number (–)
T	time (s)
T	temperature (K)
u, **u**	continuous and discrete input vector
v, v_F	velocity (m/s), velocity at flame base (m/s)
W	convective forcing velocity (m/s)
$\mathcal{W}$	continuous energy weighting operator
x, **x**	continuous and discrete state vector
X	Set of spatial variables ξ
y, **y**	continuous and discrete output vector
α	flame angle ($^\circ$)
β	non-dimensional spatial profile of temperature (–)
γ	heat capacity ratio (–)
δ_{ξ_F}	Dirac measure for heat addition to acoustic field (–)
Δ_β	temperature incremental factor across heat source (–)
ζ	damping coefficient (1/s)
κ	ratio of kernel to output energy (–)
μ	ratio of convective to mean flow velocity w/v_0 (–)
ξ,ξ_F	spatial variable (m), flame position (m)
Π	ratio of convective to restorative time scale τ_c/τ_r (–)
ρ	density (kg/m^3)
Σ	entropy [J/(kg K)]
τ	history (s)
τ_c,τ_r	characteristic time scale of convective forcing and of restoration (s)
ϕ	Equivalence/fuel-to-air ratio (–)
Φ	dummy function (–)
$\partial\Omega$	outer boundary
Ω	volume (m^3)

Subscripts

0	mean quantity or at initial time t_0
A	acoustics/flow subsystem
crit	at the linear stability bound
F	flame subsystem
max	maximum
N	total state energy
U	upstream

Superscripts

*	optimal
†	kernel
T	transformed

Appendix 1. Deriving the non-dimensional set of governing equations

The dimensional set of equations governing the respective conservation of momentum and of energy and mass read

$$\frac{\partial \tilde{v}}{\partial \tilde{t}} = -\tilde{v}_0 \frac{\partial \tilde{v}}{\partial \tilde{\xi}} - \tilde{v} \frac{\partial \tilde{v}_0}{\partial \tilde{\xi}} + \tilde{\zeta}_v \tilde{v} - \frac{1}{\tilde{\rho}_0} \frac{\partial \tilde{p}}{\partial \tilde{\xi}} \tag{39(a)}$$

$$\frac{\partial \tilde{p}}{\partial \tilde{t}} = -\gamma \tilde{p}_0 \frac{\partial \tilde{v}}{\partial \tilde{\xi}} - \tilde{v}_0 \frac{\partial \tilde{p}}{\partial \tilde{\xi}} - \gamma \tilde{p} \frac{\partial \tilde{v}_0}{\partial \tilde{\xi}} + K_0 \frac{(\gamma - 1)}{\tilde{A}_A} \tilde{\dot{q}}\, \tilde{d} \tag{39(b)}$$

where $\tilde{}$ denotes dimensional quantities. With the reference scales given in equation (9), equation (39) can be transformed to express the non-dimensional temporal evolution of acoustic velocity and pressure, respectively. Keeping in mind that the speed of sound $\tilde{c}_0 = \tilde{c}_0(\tilde{\xi})$ is a function of space, and with the definitions of β, M and K as given in equation (10) to (12), respectively, equation (39) becomes

$$\frac{\partial v}{\partial t} = -M \frac{\partial v}{\partial \xi} - \left(2 \frac{M}{\beta} \frac{\partial \beta}{\partial \xi} + \frac{\partial M}{\partial \xi} - \zeta_v \right) v - \frac{\partial p}{\partial \xi} \tag{40(a)}$$

$$\frac{\partial p}{\partial t} = -\frac{\partial v}{\partial \xi} - \frac{1}{\beta} \frac{\partial \beta}{\partial \xi} v - M \frac{\partial p}{\partial \xi} - \left(\gamma \frac{\partial M}{\partial \xi} + \gamma \frac{M}{\beta} \frac{\partial \beta}{\partial \xi} - \zeta_p \right) p + K \dot{q}\, d \tag{40(b)}$$

From equations (10) and (11), we find that $M(\xi) = M_u\, \beta(\xi)$, which substituted into equation (40) yields the non-dimensional governing equations shown in equation (8).

Appendix 2. The discrete model of the acoustics/flow subsystem

In the following, we introduce a method that uses a variational formulation to approximate the governing state equation of the acoustics subsystem. It is very similar to FE methods and widely spread under the name of Galerkin method (to name but a few examples in thermoacoustic literature[13,15,37]). However, in recent historical overviews of the method,[59,60] Culick argues that the full breadth and universal character of the method reaches far beyond Galerkin's intentions. We follow Culick's line of arguments, and refer to the method as MWR.

The variational formulation of the MWR starts from the partial differential state equation (1(a)) governing the acoustics/flow subsystem

$$\int_0^1 (\dot{x}_A - \mathcal{A}_A\, x_A - \mathcal{B}_A\, u_A)\ \mathrm{d}\xi = 0 \tag{41}$$

The state variables are projected onto spatial basis functions $T_{A,j}(\xi)$

$$x_A = \sum_{j=1}^{N_A} x_{A,j}(t)\, T_{A,j}(\xi) = \mathcal{T}_A\, \mathbf{x}_A \tag{42}$$

which amounts to a time–space decoupling state transformation of the continuous acoustic state vector $x_A(\xi, t)$ to the discrete state vector of the MWR $\mathbf{x}_A(t)$. The columns of $\mathcal{T}_A$ contain the spatial basis functions $T_{A,j}$. Substituting equation (42) into equation (41) and multiplying by test functions $T_{A,k}(\xi)$—which are chosen as the same as the basis functions (this step is sometimes referred to as the Galerkin choice)—leads to an ordinary differential state equation for $\mathbf{x}_A$

$$\left(\int_0^1 \mathcal{T}_A \mathcal{T}_A\ \mathrm{d}\xi \right) \dot{\mathbf{x}}_A = \left(\int_0^1 (\mathcal{A}_A \mathcal{T}_A)\, \mathcal{T}_A\ \mathrm{d}\xi \right) \mathbf{x}_A + \left(\int_0^1 (\mathcal{B}_A \mathcal{T}_A)\ \mathrm{d}\xi \right) u_A \tag{43}$$

The partial differential operators $\mathcal{A}_A$ and $\mathcal{B}_A$ hence operate on known spatial expansion functions $T_{A,j}$. Equation (43) can then be brought to the form of a discrete SSM of the form of equation (5)

$$\dot{\mathbf{x}}_A = \mathbf{A}_A\, \mathbf{x}_A + \mathbf{B}_A\, \mathbf{u}_A \tag{44(a)}$$

$$\mathbf{y}_A = \mathbf{C}_A\, \mathbf{x}_A \tag{44(b)}$$

with $\mathbf{u}_A = \dot{q}$ and $\mathbf{y}_A = v_F$ as defined above.

The crucial step consists in selecting adequate expansion functions, so as to minimize the residual of the approximation equation (43) (from which the name of the method). Although not mandatory in principle, it is useful to base the choice on physical considerations of the problem under investigation. For the primitive acoustic variables v and p, it is convenient to use the mode shapes of the fundamental acoustic duct problem without mean flow, temperature jump and heat source

as expansion functions

$$v(\xi,t)=\sum_{j=1}^{N_A}\cos(j\pi\xi)\,v_{A,j}(t) \tag{45(a)}$$

$$p(\xi,t)=\sum_{j=1}^{N_A}\sin(j\pi\xi)\,p_{A,j}(t) \tag{45(b)}$$

so

$$\mathcal{T}_A=\begin{bmatrix}\cos(\pi\xi) & \cos(2\pi\xi) & \cdots & \cos(N_A\pi\xi)\\ \sin(\pi\xi) & \sin(2\pi\xi) & \cdots & \sin(N_A\pi\xi)\end{bmatrix} \tag{46}$$

and

$$\begin{aligned}\mathbf{x}_A=[\,&v_{A,1}(t)\,,\ v_{A,2}(t)\,,\ \cdots,\ v_{A,N_A}(t)\\ &p_{A,1}(t)\,,\ p_{A,2}(t)\,,\ \cdots,\ p_{A,N_A}(t)\,]^T\end{aligned} \tag{47}$$

The main benefit is that these expansion functions implicitly fulfill the boundary conditions at the duct ends, $p=0$ and $\partial v/\partial\xi\approx 0$ at $\xi=0$ and $\xi=1$. The boundary condition for v is a good approximation for low Mach numbers, as $\partial v/\partial\xi=-M\,\partial p/\partial\xi$, see equation (8(b)). Additional flux terms at the boundaries are thus not needed. The corresponding set of discrete matrices $(\mathbf{A}_A,\mathbf{B}_A,\mathbf{C}_A)$ is given in Appendix. 3. The acoustics/flow subsystem being single input single output (SISO), the continuous and discrete input and output are the same, $\mathbf{u}_A=u_A=\dot{q}$, and $\mathbf{y}_A=y_A=v_F$.

Since the acoustic field is modally expanded, the MWR provides for a unique possibility to implement frequency-dependent damping in the time domain. We use a damping correlation proposed by Matveev and Culick,[61] where damping increases with frequency

$$\zeta_v=0,\quad\text{and}\quad\zeta_p=\zeta_{p,j}=\zeta_1 j+\zeta_2\sqrt{\frac{1}{j}} \tag{48}$$

This *modal damping model* and variants thereof are widely used in the thermoacoustic community (e.g. see literatures[13,15,62, 63]). The damping coefficients ζ_1 and ζ_2 model the effects of dissipation at the duct ends and in the boundary layer, respectively. According to Kashinath,[52] typical values for laboratory-scale Rijke tubes are $\zeta_1\approx-0.01\ldots-0.13$ and $\zeta_2\approx-0.005\ldots-0.03$.

Appendix 3. Matrices of the discrete models

The acoustics/flow subsystem

The MWR is introduced in Appendix 2. The corresponding matrices of the discrete model read

$$\mathbf{A}_A=\begin{bmatrix}\mathbf{A}_{A,v_A\to v_A} & \mathbf{A}_{A,p_A\to v_A}\\ \mathbf{A}_{A,v_A\to p_A} & \mathbf{A}_{A,p_A\to p_A}\end{bmatrix},\quad\in\mathbb{R}^{(2N_A)\times(2N_A)} \tag{49}$$

$$(\mathbf{B}_A)_m=\begin{cases}2\,K\sin((m-N_A)\pi\xi_F) & \text{for } m\in[(N_A+1);2N_A]\\ 0 & \text{otherwise}\end{cases}\quad\in\mathbb{R}^{(2N_A)} \tag{50}$$

$$(\mathbf{C}_A)_n=\begin{cases}\cos(n\pi\xi_F) & \text{for } n\in[1;N_A]\\ 0 & \text{otherwise}\end{cases},\quad\in\mathbb{R}^{(2N_A)} \tag{51}$$

where

$$\left(\mathbf{A}_{A,v_A\to v_A}\right)_{mn}=2M_u\,(n\pi\mathbf{N}_{mn}-3\Delta_\beta\,\mathbf{P}_{mn})+\zeta_v\,\delta_{mn} \tag{52}$$

$$\left(\mathbf{A}_{A,p_A\to v_A}\right)_{mn}=-m\pi\,\delta_{mn} \tag{53}$$

$$\left(\mathbf{A}_{A,v_A\to p_A}\right)_{mn}=m\pi\,\delta_{mn}-\frac{2\Delta_\beta}{1+\Delta_\beta}\,\mathbf{Q}_{mn} \tag{54}$$

$$\left(\mathbf{A}_{A,p_A\to p_A}\right)_{mn}=-2M_u\,(n\pi\mathbf{N}_{nm}+2\gamma\Delta_\beta\mathbf{R}_{mn})+\zeta_p\,\delta_{mn} \tag{55}$$

for $m,n\in[1;N_A]$ and with Kronecker delta δ_{mn}. The auxiliary operators of the MWR are defined as

$$\mathbf{N}_{mn}=\begin{cases}\dfrac{\Delta_\beta}{4m\pi}\,\{\cos(2m\pi\xi_F)-1\} & \text{for } n=m\\ \dfrac{1}{\pi(n-m)(n+m)}\\ \quad\{n\,(1-\cos(n\pi)\,\cos(m\pi))\\ \quad+\Delta_\beta\,[m\,\sin(n\pi\xi_F)\,\sin(m\pi\xi_F)\\ \quad+n\,(\cos(n\pi\xi_F)\,\cos(m\pi\xi_F)\\ \quad-\cos(n\pi)\,\cos(m\pi))]\} & \text{for } n\neq m\end{cases} \tag{56}$$

and

$$\mathbf{P}_{mn}=\begin{cases}\cos^2(m\pi\xi_F) & \text{for } n=m\\ \cos(n\pi\xi_F)\,\cos(m\pi\xi_F) & \text{for } n\neq m\end{cases} \tag{57}$$

$$\mathbf{Q}_{mn} = \begin{cases} \frac{1}{2}\sin(2m\pi\xi_F) & \text{for } n = m \\ \cos(n\pi\xi_F)\,\sin(m\pi\xi_F) & \text{for } n \neq m \end{cases} \tag{58}$$

$$\mathbf{R}_{mn} = \begin{cases} \sin^2(m\pi\xi_F) & \text{for } n = m \\ \sin(n\pi\xi_F)\,\sin(m\pi\xi_F) & \text{for } n \neq m \end{cases} \tag{59}$$

The flame subsystem

The matrices of the discrete model describing the flame subsystem defined in The flame subsystem section are defined in the following. They read

$$\mathbf{A}_F = (\mathbf{M}_{\mathrm{FE}})^{-1}\,\mathbf{K}_{\mathrm{FE}}, \quad \in \mathbb{R}^{N_F \times N_F} \tag{60}$$

$$\mathbf{B}_F = (\mathbf{M}_{\mathrm{FE}})^{-1}\,\mathbf{B}_{\mathrm{FE}}, \quad \in \mathbb{R}^{N_F} \tag{61}$$

$$\mathbf{C}_F = \Delta\tau\check{h}, \quad \in \mathbb{R}^{N_F} \tag{62}$$

with discrete impulse response function $\check{h}$ and finite element mass and stiffness matrices, respectively

$$\mathbf{M}_{\mathrm{FE}} = \frac{\Delta\tau}{6}\begin{bmatrix} 4 & 1 & & & & & & & \\ 1 & 4 & 1 & & & & & & \\ & 1 & 4 & 1 & & & & & \\ & & \ddots & \ddots & \ddots & & & & \\ & & & & 1 & 4 & 1 & & \\ & & & & & 1 & 4 & 1 & \\ & & & & & & 1 & 2 \end{bmatrix}, \quad \in \mathbb{R}^{N_F \times N_F} \tag{63}$$

$$\mathbf{K}_{\mathrm{FE}} = \frac{1}{2\,\mathrm{Sr}}\begin{bmatrix} 0 & -1 & & & & & & & \\ 1 & 0 & -1 & & & & & & \\ & 1 & 0 & -1 & & & & & \\ & & & \ddots & \ddots & \ddots & & & \\ & & & & 1 & 0 & -1 & & \\ & & & & & 1 & 0 & -1 & \\ & & & & & & 1 & -1 \end{bmatrix}, \quad \in \mathbb{R}^{N_F \times N_F} \tag{64}$$

The full thermoacoustic system

The output matrix of the full thermoacoustic model reads

$$\mathbf{C} = [\mathbf{C}_1\ \mathbf{0}], \quad \in \mathbb{R}^{(2N_A)\times(2N_A+N_F)} \tag{65}$$

with

$$\mathbf{C}_1 = \mathrm{chol}\left(\frac{1}{4}\begin{bmatrix} \mathbf{I} & 2M_u\mathbf{N} \\ 2M_u\mathbf{N}^T & \mathbf{I} \end{bmatrix}\right), \quad \in \mathbb{R}^{(2N_A)\times(2N_A)} \tag{66}$$

and null matrix $\mathbf{0} \in \mathbb{R}^{N_A \times N_F}$, identity matrix $\mathbf{I} \in \mathbb{R}^{N_A \times N_A}$, and $\mathbf{N}$ as defined in equation (56).